NASA TECHNICAL MEMORANDUM

N73-31926
NASA TM X-2902

NASA TM X-2902

EXPERIMENTAL INVESTIGATION OF BOUNDARY LAYERS IN AN AXISYMMETRIC, MACH 2.5, MIXED-COMPRESSION INLET

by Warren R. Hingst and David F. Johnson

Lewis Research Center
Cleveland, Ohio 44135

NATIONAL AERONAUTICS AND SPACE ADMINISTRATION • WASHINGTON, D. C. • OCTOBER 1973

1. Report No.	2. Government Accession No.	3. Recipient's Catalog No.
NASA TM X-2902		

4. Title and Subtitle	5. Report Date
EXPERIMENTAL INVESTIGATION OF BOUNDARY LAYERS IN AN AXISYMMETRIC, MACH 2.5, MIXED-COMPRESSION INLET	October 1973
	6. Performing Organization Code

7. Author(s)	8. Performing Organization Report No.
Warren R. Hingst and David F. Johnson	E-7380
	10. Work Unit No. 501-24
9. Performing Organization Name and Address Lewis Research Center National Aeronautics and Space Administration Cleveland, Ohio 44135	11. Contract or Grant No.
	13. Type of Report and Period Covered Technical Memorandum
12. Sponsoring Agency Name and Address National Aeronautics and Space Administration Washington, D.C. 20546	14. Sponsoring Agency Code

15. Supplementary Notes

16. Abstract

An experimental investigation has been made of the boundary layer flow in a supersonic axisymmetric inlet. The inlet was designed for Mach 2.5 and had a 60 percent internal supersonic area contraction. Porous bleed regions were incorporated into both the cowl and centerbody for boundary-layer control. Five bleed configurations were studied; these included bleed regions upstream of, across, and downstream of the experimentally determined shock-impingement points. The tests were conducted at tunnel unit Reynolds numbers of 8.2×10^6 and 2.7×10^6 per meter. Static-pressure measurements were made along the internal inlet surfaces. In addition to locating the position of the shocks, these measurements also showed local regions of expansion resulting from the suction bleed. Boundary-layer profiles were measured with translating pitot pressure probes located on both sides of the shock-impingement points on the cowl and centerbody. These measurements showed that the boundary-layer profiles were distorted in the vicinity of the terminal shock.

17. Key Words (Suggested by Author(s))

Inlet
Supersonic
Boundary layers
Bleed
Experimental

18. Distribution Statement

Unclassified - unlimited

19. Security Classif. (of this report)	20. Security Classif. (of this page)	21. No. of Pages	22. Price*
Unclassified	Unclassified	33	Domestic, $3.00 Foreign, $5.50

* For sale by the National Technical Information Service, Springfield, Virginia 22151

EXPERIMENTAL INVESTIGATION OF BOUNDARY LAYERS IN AN AXISYMMETRIC, MACH 2.5, MIXED-COMPRESSION INLET

by Warren R. Hingst and David F. Johnson

Lewis Research Center

SUMMARY

An experimental investigation has been made of the boundary-layer flow in a supersonic axisymmetric inlet. The inlet was designed for Mach 2.5 and had a 60 percent internal supersonic area contraction. Porous bleed regions were incorporated into both the cowl and centerbody for boundary-layer control. Five bleed configurations were studied; these included bleed regions upstream of, across from, and downstream of the experimentally determined shock-impingement points. The tests were conducted at tunnel unit Reynolds numbers of 8.2×10^6 and 2.7×10^6 per meter.

Static pressure measurements were made along the internal inlet surfaces. In addition to locating the position of the shocks, these measurements also showed local regions of expansion resulting from the suction bleed. Boundary-layer profiles were measured with translating pitot pressure probes located on both sides of the shock-impingement points on the cowl and centerbody. These measurements showed that the boundary-layer profiles were distorted in the vicinity of the terminal shock.

INTRODUCTION

To accurately predict supersonic inlet performance, an understanding of both the qualitative and quantative behavior of the boundary-layer flow is essential. In addition to the ability to determine boundary-layer growth, a knowledge of the specialized problems of shock - boundary-layer interaction and boundary layer bleed are also necessary. In a supersonic inlet a bleed system is used to avoid excessive boundary-layer growth and/or flow separation, which would result in loss of pressure recovery and increased flow distortion. Although boundary-layer bleed improves inlet performance, a drag is associated with the bleed, making it desirable

to use the minimum amount of bleed. The optimization technique, therefore, involves the balancing of the improved inlet performance against the loss associated with the bleed drag.

An extensive bleed optimization investigation was performed on an axisymmetric mixed-compression inlet as reported in reference 1. The purpose of that investigation was to evaluate several bleed locations and bleed flow rates to determine their effects on inlet performance. In addition, other investigations have been made of shock - boundary-layer interactions on flat plates and tunnel walls. These include tests without bleed as reported in references 2 and 3 and with bleed as in references 4 and 5.

The present investigation is a boundary-layer study of the same axisymmetric mixed-compression inlet reported on in reference 1. The objective in this study is to determine the boundary-layer flow in an actual inlet flow environment with sufficient detail to aid in the development of analytical methods. These boundary-layer measurements combined with the bleed optimization results of reference 1 could prove useful in establishing bleed criteria.

The inlet-bleed configurations used for this investigation were selected from reference 1. The tests were conducted in the Lewis 10 by 10 Foot Supersonic Wind Tunnel at Mach 2.498 and two unit Reynolds numbers of 8.2×10^6 and 2.7×10^6 per meter. Pitot pressure surveys of the boundary layer flows were made upstream and downstream of the shock-boundary layer interactions. Static pressures were measured along the cowl and centerbody surfaces. In addition, the bleed flow rates were recorded for both the cowl and centerbody bleed systems. Measurements were made in English units and converted to SI units for this report.

SYMBOLS

M	Mach number
m_b/m_o	ratio of bleed to capture mass flow
P	total pressure
p	static pressure
R_c	inlet capture radius, 0.2366 m
Re	Reynolds number
r	radius
T	total temperature

t	temperature
x	axial distance from spike tip
y	distance normal to inlet surface
α	angular location

Subscripts:

b	bleed
e	boundary-layer edge
0	free stream
p	plenum
w	wall

APPARATUS AND PROCEDURE

An axisymmetric mixed-compression inlet designed for Mach 2.50 was used in this investigation. At the design Mach number, 40 percent of the supersonic flow area contraction was external and 60 percent was internal. The inlet had a capture area of 0.1758 square meter and was attached to a cylindrical nacelle 0.635 meter in diameter. The inlet was installed to a cold-pipe choked-exit plug assembly. Figure 1 is a photograph of the inlet-nacelle combination mounted in the wind tunnel test section.

Details of the inlet design are shown in table I and figures 2 and 3. External compression was accomplished with a 12.5° half-angle cone, which remained conical to the internal inlet station x/R_c of 2.88. At the design Mach number of 2.5 the oblique shock generated by the cone passed immediately ahead of the cowl lip. The initial internal cowl lip angle was 0°. This produced an internal shock, which reflected from the centerbody and the cowl before reaching the throat region of the inlet in the vicinity of its second centerbody reflection. The inlet was designed to include additional isentropic compression. Theoretical shock impingement points computed by the inviscid method of reference 6 were at x/R_c of 2.88 and 3.475 on the centerbody and 3.25 on the cowl. The geometric throat, which was 5.75 centimeters across the annulus, was located at x/R_c of 3.475 on the centerbody, where the theoretical average supersonic Mach number was 1.239. Table I gives the inlet contour in equation form, and figure 2 shows the predicted Mach number and the ratio of local to free-stream static pressure on the cowl and centerbody surfaces.

Additional details of the inlet design are shown in figure 3. The centerbody was

supported by three equally spaced struts that provided ducting for the bleed flow. The inlet also contained two bypass systems. However, during this investigation the systems were not used. Figure 3(a) also shows the actuating mechanisms for translating the centerbody that were used to facilitate an inlet start. The total length of the inlet from the cone tip to compressor face was 7.72 cowl lip radii.

To control the shock - boundary-layer interaction, the inlet design included four porous bleed regions (shown in figs. 3(b) and (c)). The bleed holes were normal to the inlet surface and were 0.3175 centimeter in diameter. The holes were equally spaced around the circumference with alternate rows staggered to provide a more uniform spatial distribution of open area. The maximum distance between hole centers for the forward bleed regions was 0.4763 centimeter. The forward cowl bleed region, located between x/R_c of 3.12 and 3.32, contained 12 rows of bleed holes; the forward centerbody bleed region, located between x/R_c of 3.31 and 3.45, contained eight rows. These regions corresponded with the cowl and second centerbody shock impingement points. Aft bleed regions were located in the inlet throat and consisted of four rows on the cowl and five rows on the centerbody. The location, the pattern and the amount of the bleed could be determined by selectively filling bleed holes. The bleed-hole arrangements and their location are shown schematically in figure 3(c) along with the theoretical and experimental shock locations.

The bleed configurations shown in figure 4 are the same as those of reference 1 and were formed by filling selected rows of holes. In relation to the shock impingement points, the bleed arrangement designated US was upstream, AS was across the shock, and those with the DS prefix were downstream. The forward and aft cowl bleeds were ducted separately and discharged overboard as shown in figure 3(b). The centerbody bleed flows were combined into a single plenum and ducted through the centerbody support struts to exits on the cylindrical portion of the nacelle. Cowl bleed flows were determined by measuring static and total pressures at a known flow exit area. The centerbody bleed flow was measured in the centerbody cavity using a similar technique.

Surface static pressures were measured along the internal inlet surface. The region where static pressure measurements were made extended from x/R_c of 2.817 to 3.743 on the cowl and from x/R_c of 2.738 to 3.755 on the centerbody. The locations of the individual pressure taps are given in table II. The pressure taps

that were located in the bleed regions are noted in the table.

Boundary-layer properties were measured by using a series of seven translating pitot pressure probes. These probes were located upstream and downstream of the shock-impingement points on both the cowl and centerbody and were capable of traversing the boundary layer in a series of predetermined steps. The boundary-layer probe locations are shown schematically in figure 5(a). The details and dimensions of the probe tip are shown in figure 5(b). Where bleed regions were associated with the shock impingements, the boundary-layer probes were located outside the immediate bleed regions. The static pressure was measured at each probe location with two surface static taps and was assumed to be uniform across the boundary layer. The probe position was corrected for shear using the technique of reference 7, which for turbulent flow compensates for the displacement of the effective center from the geometric center towards the region of higher velocity. The inlet wall temperature was recorded at each probe location. Figure 5(c) is a photograph showing the boundary layer probes installed in the inlet.

RESULTS AND DISCUSSION

The results of the investigation are presented as a study of boundary-layer phenomena with shock interaction and bleed; that is, the overall performance of the inlet will not be discussed, since reference 1 presents these results for the inlet under very similar test conditions. Therefore, the data presented here will consist of surface pressure measurements, boundary-layer Mach number profiles and bleed rates. In addition, the wall and edge conditions are given for each boundary-layer profile.

Table III presents for each reading number a summary of the test conditions, the ratio of bleed mass flow to total inlet mass flow and the bleed plenum pressure for each bleed system. In addition, for each probe the wall temperature and boundary-layer edge Mach number, total temperature, and total pressure are given.

The ratio of surface static pressure to free-stream total pressure along the cowl and centerbody for the 2.6×10^6 per meter Reynolds number conditions is shown in figures 6 to 10. The pressure ratios are shown for each bleed configuration with the inlet operating with the terminal shock at three axial locations, where A, B, and C denote progressively downstream positions. In general, the cowl pressures indicate that for operation at mode A the terminal shock pressure rise reached the oblique

impingment point on the cowl. For operation at modes B and C the cowl pressures show the initial oblique shock pressure increase followed by a short expansion and the terminal shock pressure rise. The expansion was associated with the concentrated bleed in these regions. The centerbody static-pressure plots also show an expansion coinciding with the bleed regions. The expansion was most pronounced for the high bleed flows of the DS III configuration.

The boundary-layer Mach number profiles for the 2.7×10^6 per meter Reynolds number conditions are presented in figures 11 to 16. The profiles on either side of the first centerbody shock interaction are given for only one bleed configuration, (US) because the change in bleed did not have any effect on this forward centerbody interaction. The profiles at probe station 1 show the boundary layer was seperated at the first shock interaction region on the centerbody. This would indicate that the boundary layer was still laminar approaching the shock interaction region. However, the flow had become reattached at probe station 2. This was the case for all bleed configurations at this Reynolds number. For peak-recovery operation at mode A where the terminal shock was furthest forward, the boundary layers were distorted in the vicinity of the terminal shock. This is most noticeable from the profiles for this case at probe 3 on the centerbody.

The ratio of surface static to free-steam total pressure for the 8.2×10^6 per meter Reynolds number condition is given in figures 17 to 21. The results are similar to those discussed previously for the lower Reynolds number. In figures 22 to 27 the Mach number profiles are presented for the five bleed configurations at a Reynolds number of 8.2×10^6 per meter. Figure 22 shows that at this Reynolds number the initial centerbody shock impingement did not separate the boundary layer as was the case for the lower Reynolds number. Mode A again produced distorted profiles in the region of the terminal shock interactions. In addition, a definite separation region occurred in the vicinity of the second centerbody interaction. These separations could result from back flow through the forward centerbody bleed for bleed configurations where large amounts of aft bleed caused high plenum pressures. This is shown in table III, where for mode A operation centerbody bleed plenum pressures are recorded equal to that of the static pressure on the forward centerbody bleed regions.

SUMMARY OF RESULTS

An investigation was conducted to obtain detailed measurements of the boundary-layer flow in an axisymmetric, mixed-compression inlet designed for Mach 2.5. The inlet had 40 percent external compression provided by a 12.5° half-angle cone. An inlet bleed system was used for boundary-layer control. The effect of the bleed location and bleed amount on the boundary layer was determined for the inlet operating at two free-stream unit Reynolds numbers, 8.2×10^6 per meter and 2.7×10^6 per meter. Surface static pressure measurements were made along the inlet surfaces and pitot pressure surveys were made through the boundary layers. From these measurements the following results were obtained:

1. The boundary-layer profiles were distorted in the vicinity of the terminal shock.

2. Boundary-layer surveys showed that for the 2.7×10^6 per meter Reynolds number case the boundary layer was apparently laminar and separated at the first centerbody shock-impingement point. The boundary layer became reattached a short distance downstream of the interaction.

3. Large bleed rates in the aft portion of the centerbody bleed region produced reverse flow through the forward bleed holes resulting in a separated boundary layer.

4. In addition to locating the shocks, the static-pressure measurements indicated regions of expansion coinciding with the bleed regions.

Lewis Research Center,
National Aeronautics and Space Administration,
Cleveland, Ohio, June 21, 1973,
501-24.

REFERENCES

1. Cubbison, Robert W.; Meleason, Edward T.; and Johnson, David F.: Effect of Porous Bleed in a High-Performance Axisymmetric, Mixed-Compression Inlet at Mach 2.50. NASA TM X-1692, 1968.
2. Pinckney, S. Z.: Data on Effects of Incident-Reflecting Shocks on the Turbulent Boundary Layer. NASA TM X-1221, 1966.

3. Kilburg, Richard F.; and Kotansky, Donald R.: Experimental Investigation of the Interaction of a Plane, Oblique, Incident-Reflecting Shock Wave with a Turbulent Boundary Layer on a Cooled Surface. General Dynamics/Fort Worth (NASA CR-66841), Oct. 1969.

4. Strike, W. T.; and Rippey, J. O.: Influence of Suction on the Interaction of an Oblique Shock with a Turbulent Boundary Layer at Mach Number 3.0. Rep. AEDC-TN-61-129, Arnold Eng. Development Center, Oct. 1961.

5. Seebaugh, W. R.; and Childs, M. E.: Conical Shock-Wave Turbulent Boundary-Layer Interaction Including Suction Effects. J. Aircraft, vol. 7, no. 4, July-Aug. 1970, pp. 334-340.

6. Sorensen, Virginia L.: Computer Program for Calculating Flow Fields in Supersonic Inlets. NASA TN D-2897, 1965.

7. MacMillan, F. A.: Experiments on Pitot-Tubes in Shear Flow. R. & M. No. 3028, Aeronautical Res. Council, Gt. Britain, 1957.

TABLE I. - INLET CONTOUR EQUATIONS

$$\left[R = a_0 + a_1 x/R_c + a_2(x/R_c)^2 + a_3(x/R_c)^3.\right]$$

a_0	a_1	a_2	a_3	Minimum axial distance, x/R_c
Centerbody coefficients				
0	0.221690	0	0	0
-.117562	-.0686815	.244819	-.0450772	2.87348
-80.1714	67.6828	-18.8490	1.74666	3.43532
9.05786	-6.37110	1.63555	-.141953	3.65003
-.549874	.972234	-.232649	.016264	4.07944
-1.00723	1.11977	-.233621	.0141971	4.72356
Cowl coefficients				
1.000	0	0	0	2.00852
.632074	.335405	-.0876992	.00493565	2.39748
.791069	.214535	-.0612318	.00366218	2.88342
6.34488	-4.24523	1.12573	-.100948	3.54267
7.37531	-4.55285	1.07795	-.0858415	3.86473
2.35019	-.869625	.178072	-.0125569	4.07944
1.34645	-8.20127	1.78457	-.0129433	4.29415
-.0518106	.641500	-.0143778	.0107363	4.56253

TABLE II. - LOCATION OF INTERNAL STATIC PRESSURE TAPS IN INLET MODELS

Cowl[a]	Centerbody	Cowl[a]	Centerbody
Axial distance, x/R_c			
2.817	[b]2.738	3.382	3.263
2.871	2.791	3.403	[b]3.296
[b]3.113	2.813	3.425	[c]3.315
[c]3.125	2.834	3.446	[c]3.332
[c]3.144	2.856	3.468	[c]3.349
[c]3.161	2.877	3.489	[c]3.367
[c]3.177	2.899	3.510	[c]3.385
[c]3.196	2.920	3.532	[c]3.402
[c]3.213	2.941	[b]3.553	[c]3.419
[c]3.230	2.963	3.674	[c]3.438
[c]3.248	2.984	3.722	3.457
[c]3.265	[b]3.027	3.743	3.478
[c]3.283	3.156		3.500
[c]3.300	3.178		3.521
[c]3.317	3.199		[b]3.543
[b]3.339	3.221		3.659
3.360	3.242		3.755

[a]Cowl lip reference $x/R_c = 2.009$.
[b]Boundary-layer probe location.
[c]Static located in porous bleed region.

TABLE III. - BOUNDARY LAYER WALL, EDGE, AND BLEED CONDITIONS

Reading	Reynolds number per meter, Re/m	Bleed	Mode	Bleed mass-flow ratio, m_b/m_b			Plenum static pressure, p_p, N/m^2			Probe number	Boundary-layer edge			Wall temperature, t_w, K
				Cowl		Centerbody	Cowl		Centerbody		Mach number, M_e	Total pressure, P_e, N/m^2	Total temperature, T_e, K	
				Forward	Aft		Forward	Aft						
77	2.7×10^6	US	A	0.02516	0.01182	0.05457	1894.8	1816.7	7490.3	1	2.09	26506.5	302.9	292.9
				0.02516	0.01182	0.05457	1894.8	1816.7	7490.3	2	1.45	25515.4	302.9	292.0
				0.02516	0.01182	0.05457	1894.8	1816.7	7490.3	3	1.10	26193.5	302.9	293.0
				0.02516	0.01182	0.05457	1894.8	1816.7	7490.3	4	0.83	25237.7	302.9	297.7
				0.02516	0.01182	0.05457	1894.8	1816.7	7490.3	5	1.49	26013.3	302.9	292.4
				0.02516	0.01182	0.05457	1894.8	1816.7	7490.3	6	0.81	26230.1	302.9	296.4
				0.02516	0.01182	0.05457	1894.8	1816.7	7490.3	7	0.84	25994.2	302.9	297.9
51			B	0.02290	0.01090	0.04131	1677.5	1833.4	5835.7	1	2.08	26204.9	299.8	299.8
				0.02290	0.01090	0.04131	1677.5	1833.4	5835.7	2	1.57	26645.4	299.8	290.1
				0.02290	0.01090	0.04131	1677.5	1833.4	5835.7	3	1.16	25199.4	299.8	291.2
				0.02290	0.01090	0.04131	1677.5	1833.4	5835.7	4	0.90	25055.7	299.8	295.6
				0.02290	0.01090	0.04131	1677.5	1833.4	5835.7	5	1.49	25568.1	299.8	290.2
				0.02290	0.01090	0.04131	1677.5	1833.4	5835.7	6	0.88	26022.9	299.8	294.2
				0.02290	0.01090	0.04131	1677.5	1833.4	5835.7	7	0.91	25663.8	299.8	295.1
52			C	0.02330	0.00680	0.03667	1716.8	1872.7	4986.0	1	2.09	26554.4	300.7	290.2
				0.02330	0.00680	0.03667	1716.8	1872.7	4986.0	2	1.62	26937.4	300.7	289.7
				0.02330	0.00680	0.03667	1716.8	1872.7	4986.0	3	1.24	26286.3	300.7	291.3
				0.02330	0.00680	0.03667	1716.8	1872.7	4986.0	4	0.95	25252.0	300.7	295.3
				0.02330	0.00680	0.03667	1716.8	1872.7	4986.0	5	1.48	25860.1	300.7	289.9
				0.02330	0.00680	0.03667	1716.8	1872.7	4986.0	6	0.90	26133.0	300.7	293.5
				0.02330	0.00680	0.03667	1716.8	1872.7	4986.0	7	0.96	25788.3	300.7	294.0
81		AS	A	0.02434	0.01998	0.06636	1844.4	2106.3	8037.8	3	1.09	25778.7	299.7	291.2
				0.02434	0.01998	0.06636	1844.4	2106.3	8037.8	4	0.81	25194.6	299.7	295.7
				0.02434	0.01998	0.06636	1844.4	2106.3	8037.8	5	1.43	24883.4	299.7	289.4
				0.02434	0.01998	0.06636	1844.4	2106.3	8037.8	6	0.81	26645.4	299.7	293.6
				0.02434	0.01998	0.06636	1844.4	2106.3	8037.8	7	0.80	25759.6	299.7	295.4
84			B	0.01826	0.01793	0.04624	1343.3	1971.1	5779.5	3	1.19	25577.6	300.7	291.8
				0.01826	0.01793	0.04624	1343.3	1971.1	5779.5	4	1.02	26008.6	300.7	295.6
				0.01826	0.01793	0.04624	1343.3	1971.1	5779.5	5	1.45	25060.5	300.7	290.2
				0.01826	0.01793	0.04624	1343.3	1971.1	5779.5	6	0.92	25912.8	300.7	293.3
				0.01826	0.01793	0.04624	1343.3	1971.1	5779.5	7	0.94	25855.3	300.7	294.5
83			C	0.01818	0.01167	0.04252	1313.2	1705.9	5320.2	3	1.19	25381.3	302.5	293.4
				0.01818	0.01167	0.04252	1313.2	1705.9	5320.2	4	1.09	25960.7	302.5	296.7
				0.01818	0.01167	0.04252	1313.2	1705.9	5320.2	5	1.45	25290.3	302.5	291.2
				0.01818	0.01167	0.04252	1313.2	1705.9	5320.2	6	0.94	26051.6	302.5	294.2
				0.01818	0.01167	0.04252	1313.2	1705.9	5320.2	7	0.98	25817.0	302.5	295.2
17		DS	A	0.01724	0.01825	0.06859	1021.3	1834.8	6551.0	3	1.19	25323.9	303.7	294.2
				0.01724	0.01825	0.06859	1021.3	1834.8	6551.0	4	0.81	24768.5	303.7	297.9
				0.01724	0.01825	0.06859	1021.3	1834.8	6551.0	5	1.48	25726.1	303.7	292.1
				0.01724	0.01825	0.06859	1021.3	1834.8	6551.0	6	0.80	25486.7	303.7	295.6
				0.01724	0.01825	0.06859	1021.3	1834.8	6551.0	7	0.84	25663.8	303.7	296.8
2			B	0.01697	0.01394	0.03762	1119.2	1801.2	4896.3	3	1.00	20698.6	300.2	290.8
				0.01697	0.01394	0.03762	1119.2	1801.2	4896.3	4	0.97	26616.6	300.2	294.4
				0.01697	0.01394	0.03762	1119.2	1801.2	4896.3	5	1.47	26626.2	300.2	289.6
				0.01697	0.01394	0.03762	1119.2	1801.2	4896.3	6	1.00	27128.9	300.2	292.1
				0.01697	0.01394	0.03762	1119.2	1801.2	4896.3	7	0.97	27320.5	300.2	293.3
15			C	0.01383	0.01225	0.03853	933.8	1589.6	4693.3	3	1.18	25137.1	303.5	293.4
				0.01383	0.01225	0.03853	933.8	1589.6	4693.3	4	0.99	25802.7	303.5	297.1
				0.01383	0.01225	0.03853	933.8	1589.6	4693.3	5	1.48	25754.8	303.5	291.5
				0.01383	0.01225	0.03853	933.8	1589.6	4693.3	6	1.00	26468.2	303.5	294.3
				0.01383	0.01225	0.03853	933.8	1589.6	4693.3	7	0.98	26367.7	303.5	295.6
30		DSI	A	0.02073	0.	0.04499	1228.3		5691.6	3	1.18	26037.3	299.2	290.1
				0.02073	0.	0.04499	1228.3		5691.6	4	0.81	25194.6	299.2	294.4
				0.02073	0.	0.04499	1228.3		5691.6	5	1.45	25673.4	299.2	287.9
				0.02073	0.	0.04499	1228.3		5691.6	6	0.82	26338.9	299.2	290.8
				0.02073	0.	0.04499	1228.3		5691.6	7	0.85	26410.7	299.2	292.9
31			B	0.01417	0.	0.02988	933.3		4186.3	3	1.17	26099.5	302.2	292.2
				0.01417	0.	0.02988	933.3		4186.3	4	0.93	25817.0	302.2	296.2
				0.01417	0.	0.02988	933.3		4186.3	5	1.47	25931.9	302.2	290.3
				0.01417	0.	0.02988	933.3		4186.3	6	0.94	26425.1	302.2	292.4
				0.01417	0.	0.02988	933.3		4186.3	7	0.94	26410.7	302.2	294.0

TABLE III. - Continued.

Reading	Reynolds number per meter, Re/m	Bleed	Mode	Bleed mass-flow ratio, m_b/m_b			Plenum static pressure, p_p, N/m^2			Probe number	Boundary-layer edge			Wall temperature, t_w, K
				Cowl		Centerbody	Cowl		Centerbody		Mach number, M_e	Total pressure, P_e, N/m^2	Total temperature, T_e, K	
				Forward	Aft		Forward	Aft						
32	2.7×10^6	DSI	C	0.01385	0.	0.03029	949.6		4117.5	3	1.16	25654.2	305.0	295.1
				0.01385	0.	0.03029	949.6		4117.5	4	0.96	26367.7	305.0	298.8
				0.01385	0.	0.03029	949.6		4117.5	5	1.47	26008.6	305.0	293.3
				0.01385	0.	0.03029	949.6		4117.5	6	0.91	25663.8	305.0	295.3
				0.01385	0.	0.03029	949.6		4117.5	7	0.96	27014.0	305.0	296.6
118		DSIII	A	0.03887	0.05371	0.08446	2682.1	5116.7	9912.0	3	1.22	25668.6	301.4	292.6
				0.03887	0.05371	0.08446	2682.1	5116.7	9912.0	4	0.82	25970.2	301.4	297.3
				0.03887	0.05371	0.08446	2682.1	5116.7	9912.0	5	1.45	24055.0	301.4	291.1
				0.03887	0.05371	0.08446	2682.1	5116.7	9912.0	6	0.72	25252.0	301.4	295.3
				0.03887	0.05371	0.08446	2682.1	5116.7	9912.0	7	0.82	26228.8	301.4	297.7
108			B	0.03452	0.05127	0.06805	2331.6	5057.2	7961.7	3	1.28	24964.8	300.4	291.2
				0.03452	0.05127	0.06805	2331.6	5057.2	7961.7	4	0.91	24782.8	300.4	294.4
				0.03452	0.05127	0.06805	2331.6	5057.2	7961.7	5	1.45	24696.6	300.4	290.3
				0.03452	0.05127	0.06805	2331.6	5057.2	7961.7	6	1.03	24825.9	300.4	294.3
				0.03452	0.05127	0.06805	2331.6	5057.2	7961.7	7	0.90	26228.8	300.4	296.4
109			C	0.03410	0.01998	0.04967	2283.2	2073.5	5481.5	3	1.25	25539.3	302.3	292.2
				0.03410	0.01998	0.04967	2283.2	2073.5	5481.5	4	1.16	25711.7	302.3	294.8
				0.03410	0.01998	0.04967	2283.2	2073.5	5481.5	5	1.43	24462.0	302.3	291.2
				0.03410	0.01998	0.04967	2283.2	2073.5	5481.5	6	1.06	24509.9	302.3	294.8
				0.03410	0.01998	0.04967	2283.2	2073.5	5481.5	7	1.13	25750.3	302.3	295.9
62	8.2×10^6	US	A	0.02234	0.01215	0.05758	5669.5	5486.7	24136.2	1	2.16	87486.8	312.9	300.3
				0.02234	0.01215	0.05758	5669.5	5486.7	24136.2	2	1.49	83062.7	312.9	301.8
				0.02234	0.01215	0.05758	5669.5	5486.7	24136.2	3	1.16	78767.8	312.9	304.7
				0.02234	0.01215	0.05758	5669.5	5486.7	24136.2	4	0.83	85653.0	312.9	310.7
				0.02234	0.01215	0.05758	5669.5	5486.7	24136.2	5	1.67	86873.9	312.9	301.9
				0.02234	0.01215	0.05758	5669.5	5486.7	24136.2	6	0.81	85461.5	312.9	307.7
				0.02234	0.01215	0.05758	5669.5	5486.7	24136.2	7	0.78	82014.1	312.9	309.5
73			B	0.02137	0.01069	0.03624	5155.2	5650.6	13905.8	1	2.16	87874.6	312.7	299.4
				0.02137	0.01069	0.03624	5155.2	5650.6	13905.8	2	1.65	88707.7	312.7	300.6
				0.02137	0.01069	0.03624	5155.2	5650.6	13905.8	3	1.51	83852.7	312.7	301.9
				0.02137	0.01069	0.03624	5155.2	5650.6	13905.8	4	0.96	82770.6	312.7	302.4
				0.02137	0.01069	0.03624	5155.2	5650.6	13905.8	5	1.68	87778.9	312.7	301.6
				0.02137	0.01069	0.03624	5155.2	5650.6	13905.8	6	0.95	85241.2	312.7	306.9
				0.02137	0.01069	0.03624	5155.2	5650.6	13905.8	7	0.98	87721.4	312.7	307.8
64			C	0.02130	0.00656	0.03139	5131.1	6150.1	12449.6	1	2.16	87467.6	312.9	299.3
				0.02130	0.00656	0.03139	5131.1	6150.1	12449.6	2	1.64	87941.7	312.9	300.4
				0.02130	0.00656	0.03139	5131.1	6150.1	12449.6	3	1.51	83407.4	312.9	301.9
				0.02130	0.00656	0.03139	5131.1	6150.1	12449.6	4	0.98	82401.9	312.9	307.9
				0.02130	0.00656	0.03139	5131.1	6150.1	12449.6	5	1.67	86720.7	312.9	301.4
				0.02130	0.00656	0.03139	5131.1	6150.1	12449.6	6	0.96	84867.7	312.9	307.2
				0.02130	0.00656	0.03139	5131.1	6150.1	12449.6	7	0.99	86591.4	312.9	307.2
93		AS	A	0.02524	0.02046	0.06948	6281.6	6229.4	26689.0	3	1.19	85571.6	313.1	305.3
				0.02524	0.02046	0.06948	6281.6	6229.4	26689.0	4	0.81	85724.8	313.1	310.5
				0.02524	0.02046	0.06948	6281.6	6229.4	26689.0	5	1.48	85466.2	313.1	302.1
				0.02524	0.02046	0.06948	6281.6	6229.4	26689.0	6	0.84	88291.2	313.1	307.6
				0.02524	0.02046	0.06948	6281.6	6229.4	26689.0	7	0.79	86993.6	313.1	310.1
94			B	0.01796	0.01870	0.03868	4363.3	5669.4	15387.5	3	1.48	81549.6	314.1	303.1
				0.01796	0.01870	0.03868	4363.3	5669.4	15387.5	4	0.99	86553.1	314.1	308.4
				0.01796	0.01870	0.03868	4363.3	5669.4	15387.5	5	1.67	86840.4	314.1	302.4
				0.01796	0.01870	0.03868	4363.3	5669.4	15387.5	6	1.17	86443.0	314.1	306.9
				0.01796	0.01870	0.03868	4363.3	5669.4	15387.5	7	0.95	87434.1	314.1	309.0
95			C	0.01794	0.01457	0.03292	4349.2	5262.8	12468.4	3	1.48	81343.8	313.7	302.3
				0.01794	0.01457	0.03292	4349.2	5262.8	12468.4	4	1.10	83750.0	313.7	306.3
				0.01794	0.01457	0.03292	4349.2	5262.8	12468.4	5	1.67	86840.4	313.7	301.8
				0.01794	0.01457	0.03292	4349.2	5262.8	12468.4	6	1.18	86620.2	313.7	305.8
				0.01794	0.01457	0.03292	4349.2	5262.8	12468.4	7	1.04	87467.6	313.7	307.3
21		DS	A	0.02342	0.01976	0.06946	4842.5	6288.4	25266.3	3	1.19	86792.5	313.5	305.4
				0.02342	0.01976	0.06946	4842.5	6288.4	25266.3	4	0.76	84949.1	313.5	311.6
				0.02342	0.01976	0.06946	4842.5	6288.4	25266.3	5	1.32	77154.2	313.5	302.7
				0.02342	0.01976	0.06946	4842.5	6288.4	25266.3	6	0.81	87118.1	313.5	307.4
				0.02342	0.01976	0.06946	4842.5	6288.4	25266.3	7	0.83	88233.7	313.5	310.1

TABLE III. - Concluded.

Reading	Reynolds number per meter, Re/m	Bleed	Mode	Bleed mass-flow ratio, m_b/m_b			Plenum static pressure, p_p, N/m^2			Probe number	Boundary-layer edge			Wall temperature, t_w, K
				Cowl		Centerbody	Cowl		Centerbody		Mach number, M_e	Total pressure, P_e, N/m^2	Total temperature, T_e, K	
				Forward	Aft		Forward	Aft						
22	8.2×10^6	DS	B	0.01560	0.01776	0.03576	3383.1	5537.0	13743.7	3	1.48	81961.4	313.9	302.8
				0.01560	0.01776	0.03576	3383.1	5537.0	13743.7	4	0.95	83905.3	313.9	309.3
				0.01560	0.01776	0.03576	3383.1	5537.0	13743.7	5	1.66	86869.1	313.9	301.9
				0.01560	0.01776	0.03576	3383.1	5537.0	13743.7	6	1.16	85911.5	313.9	306.2
				0.01560	0.01776	0.03576	3383.1	5537.0	13743.7	7	0.95	87515.5	313.9	308.5
23			C	0.01550	0.01188	0.02953	3420.5	4838.5	11555.2	3	1.48	82033.2	315.2	303.7
				0.01550	0.01188	0.02953	3420.5	4838.5	11555.2	4	1.05	84168.7	315.2	281.6
				0.01550	0.01188	0.02953	3420.5	4838.5	11555.2	5	1.65	85911.5	315.2	303.3
				0.01550	0.01188	0.02953	3420.5	4838.5	11555.2	6	1.17	86055.2	315.2	307.1
				0.01550	0.01188	0.02953	3420.5	4838.5	11555.2	7	1.01	87376.7	315.2	308.8
40		DSI	A	0.02436	0.	0.05419	4972.7		19943.9	3	1.18	86261.1	314.1	305.4
				0.02436	0.	0.05419	4972.7		19943.9	4	0.76	85284.3	314.1	311.7
				0.02436	0.	0.05419	4972.7		19943.9	5	1.28	76637.1	314.1	302.6
				0.02436	0.	0.05419	4972.7		19943.9	6	0.80	86399.9	314.1	306.6
				0.02436	0.	0.05419	4972.7		19943.9	7	0.80	88205.0	314.1	309.6
41			B	0.01529	0.	0.02123	3437.6		9597.0	3	1.48	82066.7	314.6	303.1
				0.01529	0.	0.02123	3437.6		9597.0	4	0.93	83685.1	314.6	309.7
				0.01529	0.	0.02123	3437.6		9597.0	5	1.65	86369.5	314.6	302.2
				0.01529	0.	0.02123	3437.6		9597.0	6	1.17	85720.0	314.6	305.4
				0.01529	0.	0.02123	3437.6		9597.0	7	0.96	87352.7	314.6	307.8
37			C	0.01529	0.	0.02074	3421.2		9341.3	3	1.48	82746.6	313.3	301.7
				0.01529	0.	0.02074	3421.2		9341.3	4	0.97	84317.1	313.3	307.9
				0.01529	0.	0.02074	3421.2		9341.3	5	1.64	86294.6	313.3	301.3
				0.01529	0.	0.02074	3421.2		9341.3	6	1.17	85932.3	313.3	304.2
				0.01529	0.	0.02074	3421.2		9341.3	7	0.98	87434.1	313.3	306.2
119		DSIII	A	0.03733	0.05455	0.08689	9054.5	20355.8	33354.0	3	1.20	83369.1	314.2	305.8
				0.03733	0.05455	0.08689	9054.5	20355.8	33354.0	4	0.80	85585.9	314.2	311.3
				0.03733	0.05455	0.08689	9054.5	20355.8	33354.0	5	1.61	84235.7	314.2	303.6
				0.03733	0.05455	0.08689	9054.5	20355.8	33354.0	6	0.67	85461.5	314.2	308.9
				0.03733	0.05455	0.08689	9054.5	20355.8	33354.0	7	0.81	86605.8	314.2	311.8
123			B	0.03367	0.05099	0.06580	7521.8	18942.9	24054.1	3	1.47	81817.8	314.5	304.2
				0.03367	0.05099	0.06580	7521.8	18942.9	24054.1	4	1.03	84930.0	314.5	308.0
				0.03367	0.05099	0.06580	7521.8	18942.9	24054.1	5	1.65	85753.5	314.5	303.4
				0.03367	0.05099	0.06580	7521.8	18942.9	24054.1	6	1.08	81894.4	314.5	308.9
				0.03367	0.05099	0.06580	7521.8	18942.9	24054.1	7	0.93	85945.0	314.5	311.2
120			C	0.03357	0.03769	0.05556	7558.3	12278.9	19863.8	3	1.48	82081.1	314.4	304.1
				0.03357	0.03769	0.05556	7558.3	12278.9	19863.8	4	1.17	85528.5	314.4	307.7
				0.03357	0.03769	0.05556	7558.3	12278.9	19863.8	5	1.65	85753.5	314.4	303.6
				0.03357	0.03769	0.05556	7558.3	12278.9	19863.8	6	1.08	81994.9	314.4	309.0
				0.03357	0.03769	0.05556	7558.3	12278.9	19863.8	7	1.21	85418.4	314.4	310.6

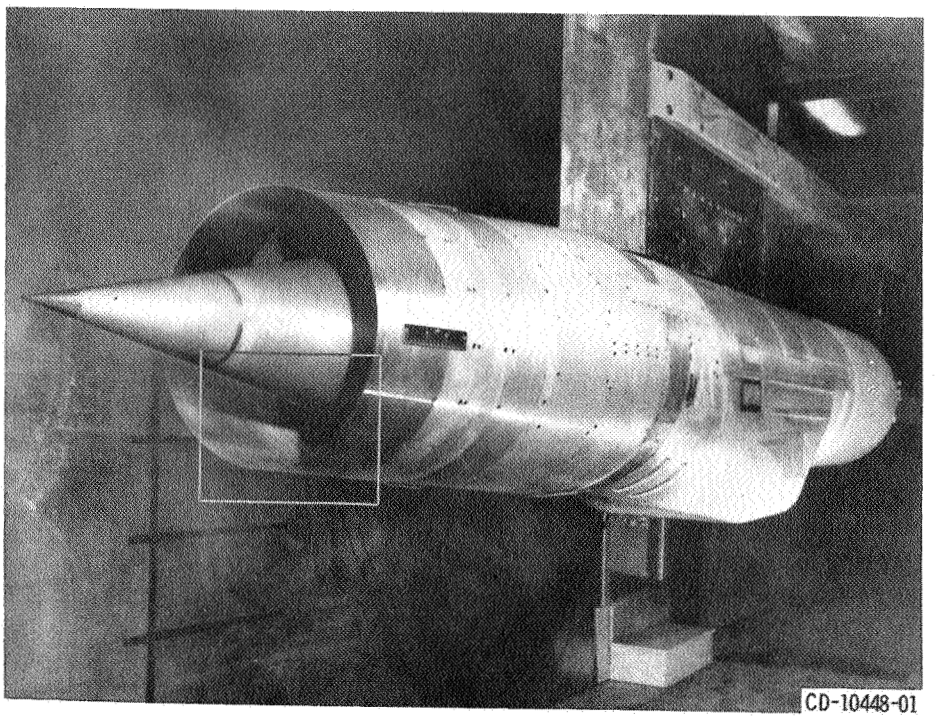

Figure 1. - Mach 2.5 mixed-compression inlet model installed in 10- by 10- Foot Supersonic Wind Tunnel test section.

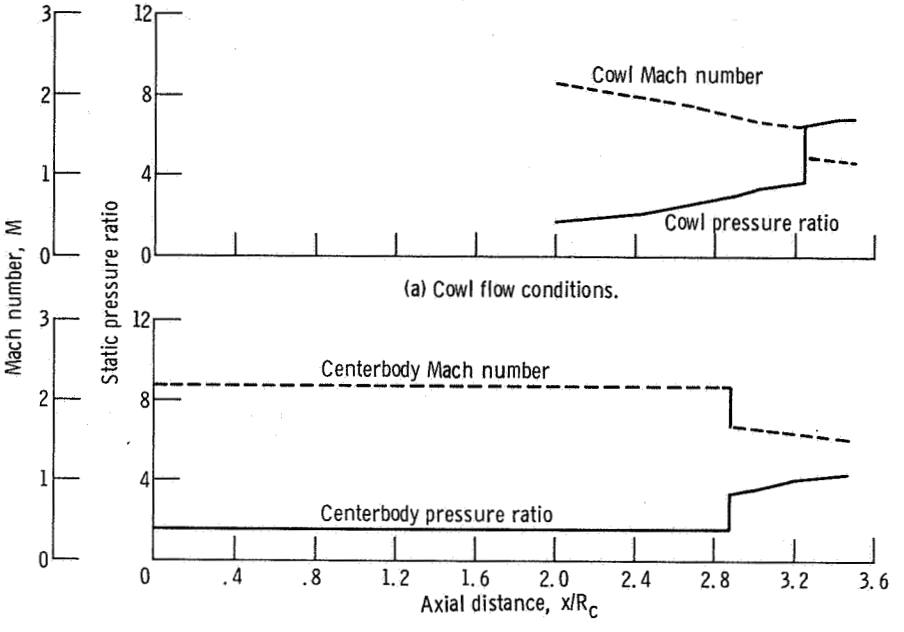

(a) Cowl flow conditions.

(b) Centerbody flow conditions.

Figure 2. - Theoretical flow conditions.

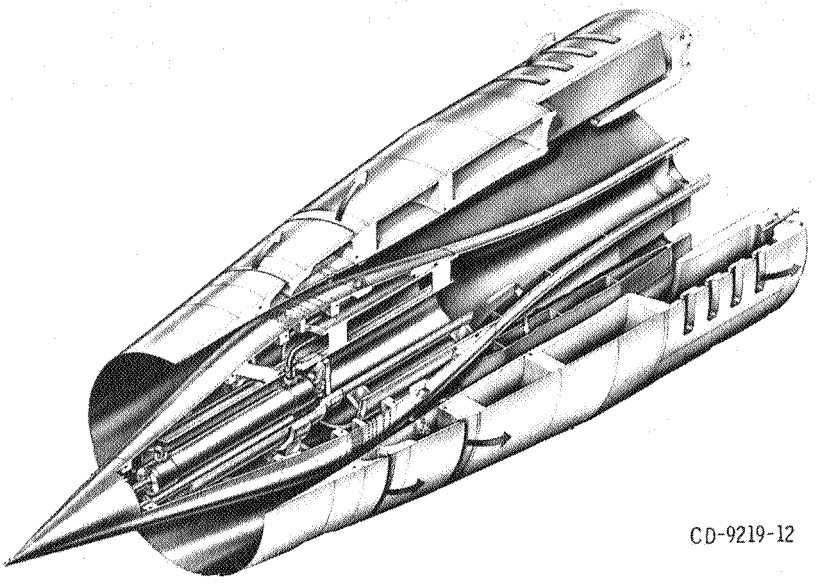

(a) Isometric view of inlet.

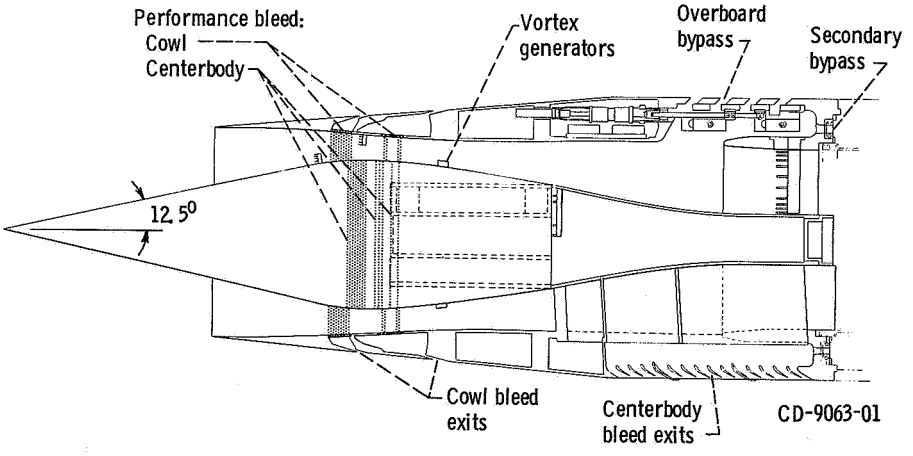

(b) Cross-section details of inlet.

Figure 3. - Inlet model details.

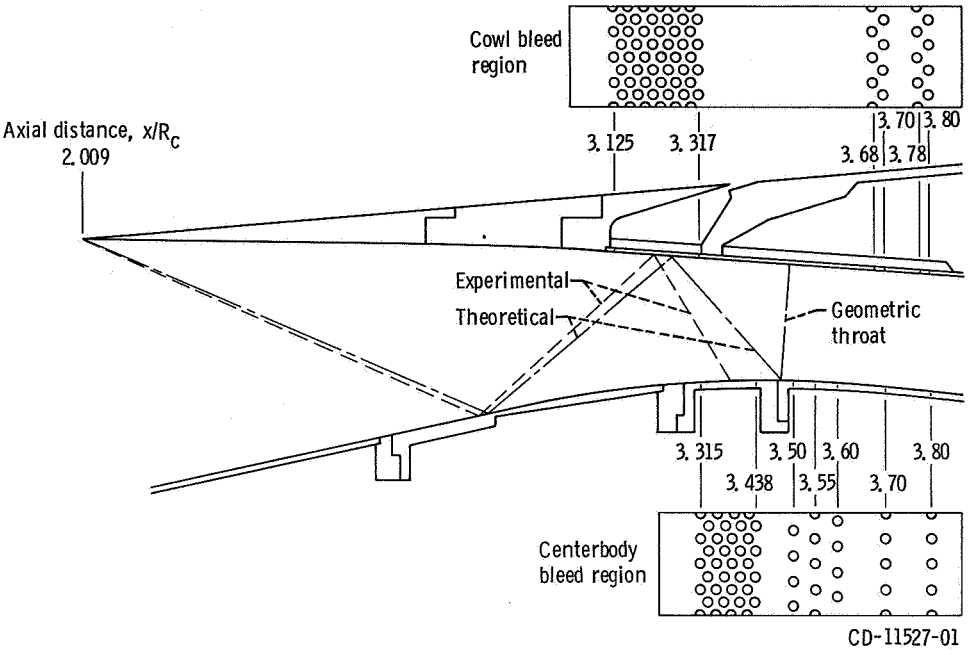

(c) Location of inlet bleed regions.

Figure 3. - Concluded.

Configuration	Cowl bleed		Centerbody bleed
	Forward	Aft	
US	○○○○○○●●●●●●	◑● ●●	○○○●●●●● ◑ ● ◑ ◑ ●
AS	●●●●○○○●●●●●	◑● ◑●	●◑○○◑●●● ◑ ◑ ◑ ◑ ●
DS	●●●●●●○○●●●●	◑● ◑●	●●●○○○◑● ◑ ◑ ◑ ◑ ●
DS-I	●●●●●●○○●●●●	●● ●●	●●●○○○◑● ● ● ● ● ●
DS-III	●●●●●●○○○○○○	○○ ○○	●●●○○○○○ ○ ○ ○ ○ ○

○ Row open
● Row closed
◑ Row alternate holes closed

Figure 4. - Locations of inlet porous bleed configurations.

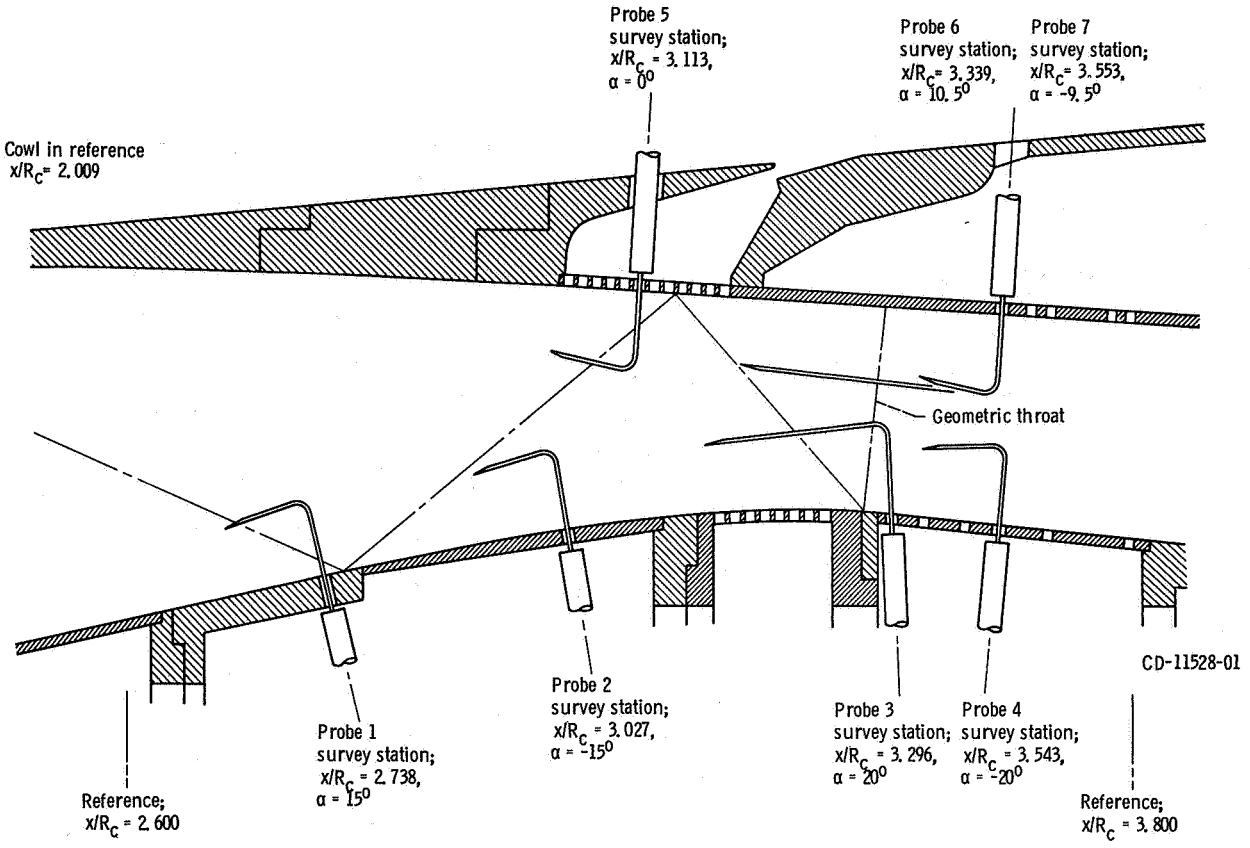

(a) Location of boundary-layer probes. Axial distance, x/R_c; angular locations of probes measured clockwise from bottom vertical centerline looking downstream.

Tubing	Outside diameter
A	0.102
B	.163
C	.229

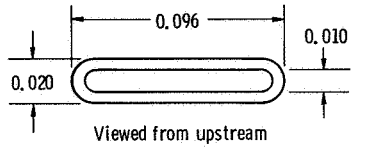

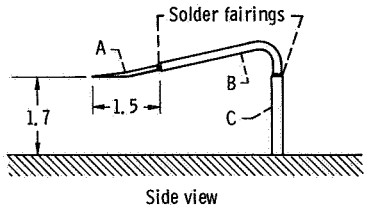

(b) Details of boundary-layer probe. (Dimensions in cm.)

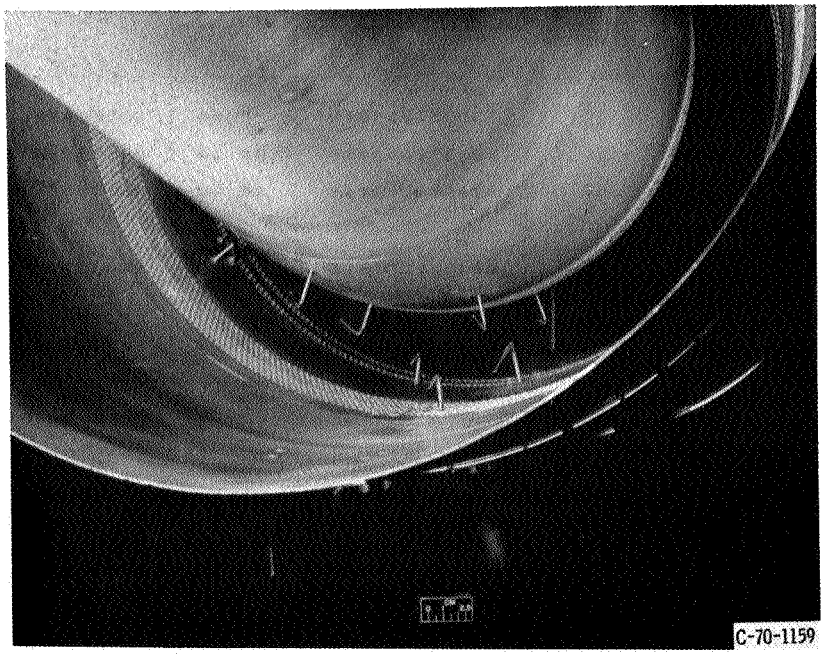

(c) Boundary layer survey instrumentation.

Figure 5. - Inlet model instrumentation.

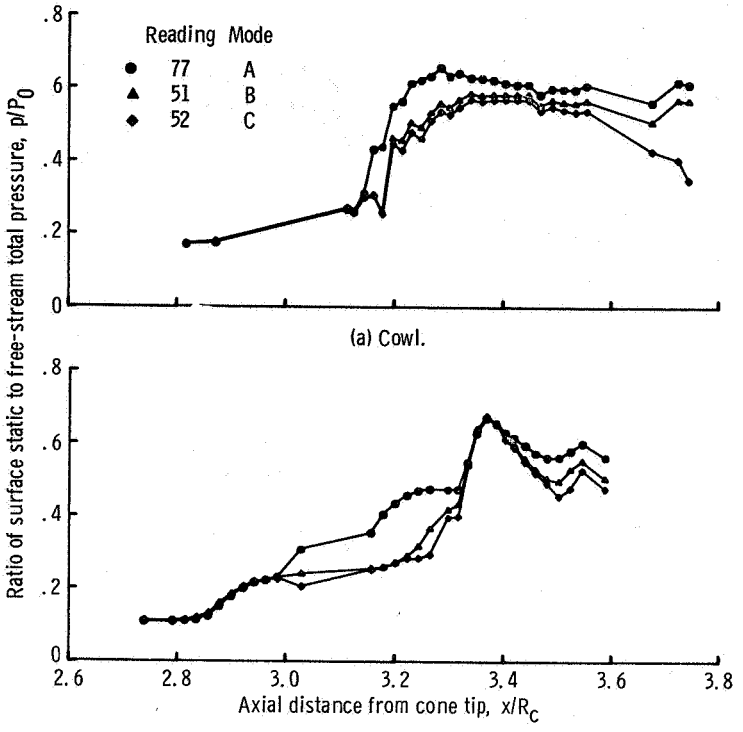

(a) Cowl.

(b) Centerbody.

Figure 6. - Static-pressure distribution for configuration US. Reynolds number per meter, 2.7×10^6.

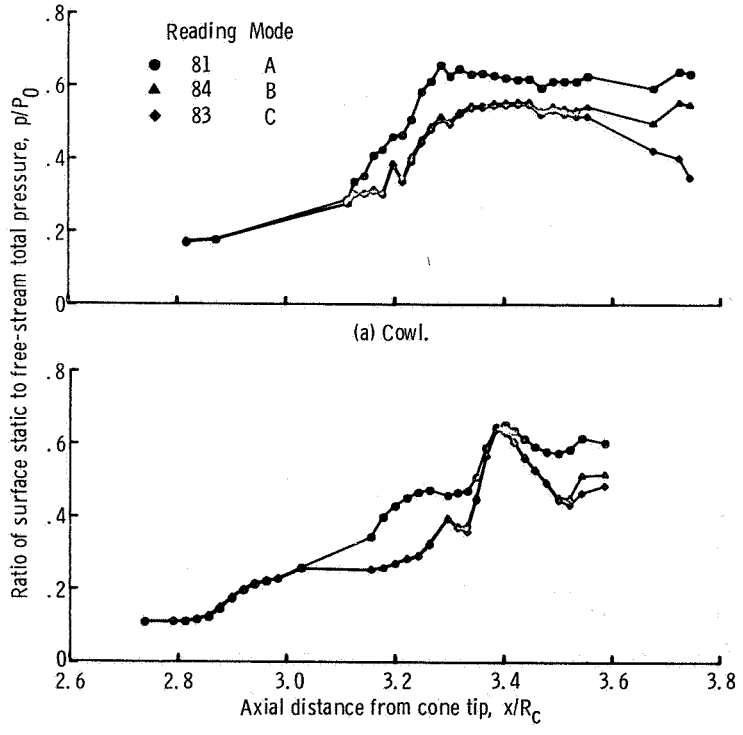

(a) Cowl.

(b) Centerbody.

Figure 7. - Static-pressure distribution for configuration AS. Reynolds number per meter, 2.7×10^6.

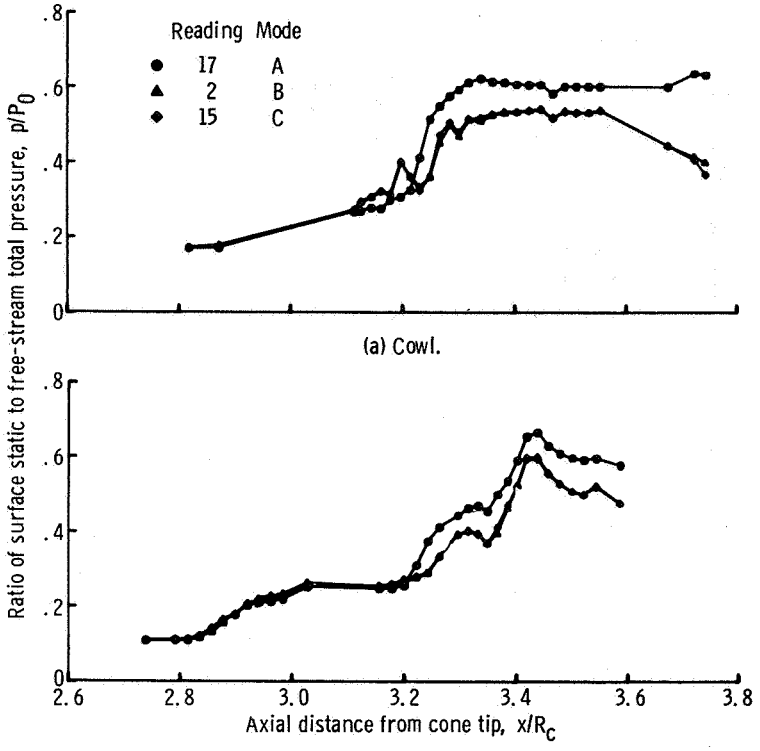

Figure 8. - Static-pressure distribution for configuration DS. Reynolds number per meter, 2.7×10^6.

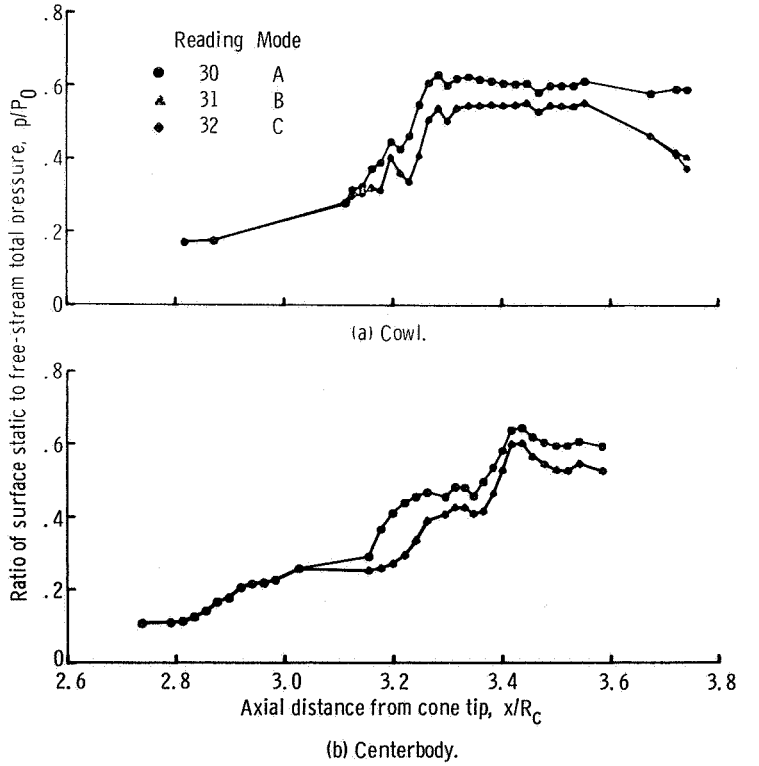

Figure 9. - Static-pressure distribution for configuration DS I. Reynolds number per meter, 2.7×10^6 m.

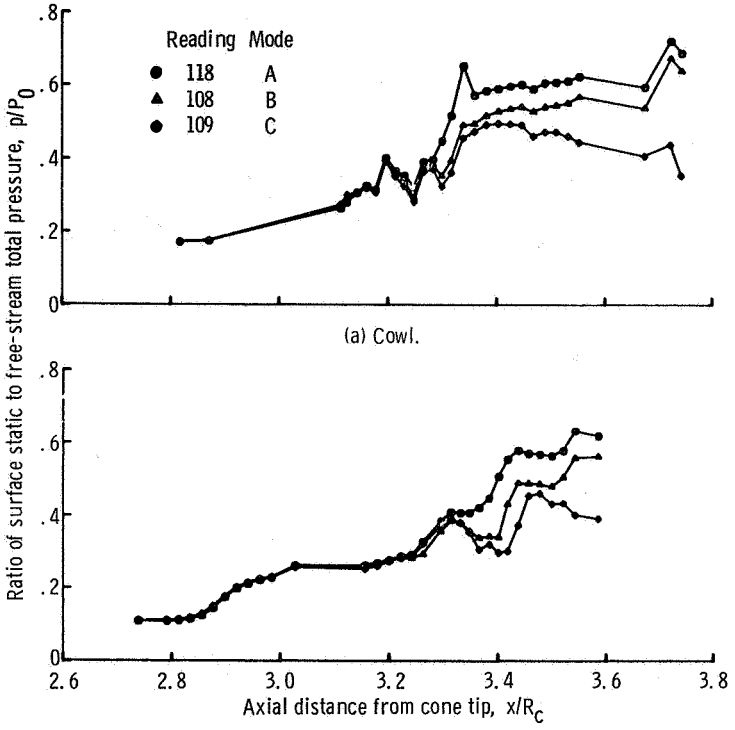

(a) Cowl.

(b) Centerbody.

Figure 10. - Static-pressure distribution for configuration DS III. Reynolds number per meter, 2.7×10^6.

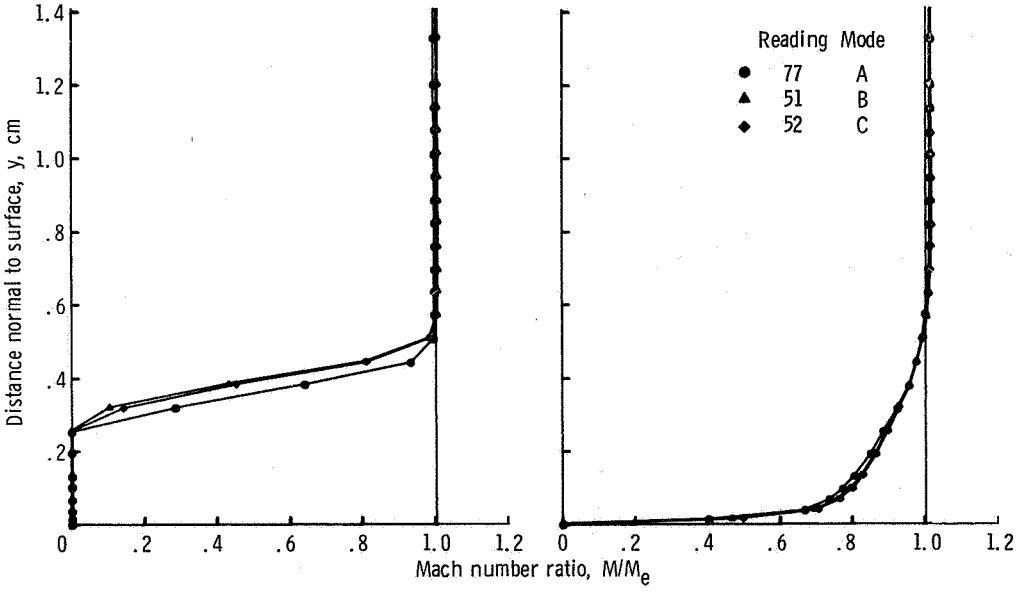

(a) Probe 1.

(b) Probe 2.

Figure 11. - Boundary-layer profiles for all bleed configurations. Reynolds number per meter, 2.7×10^6.

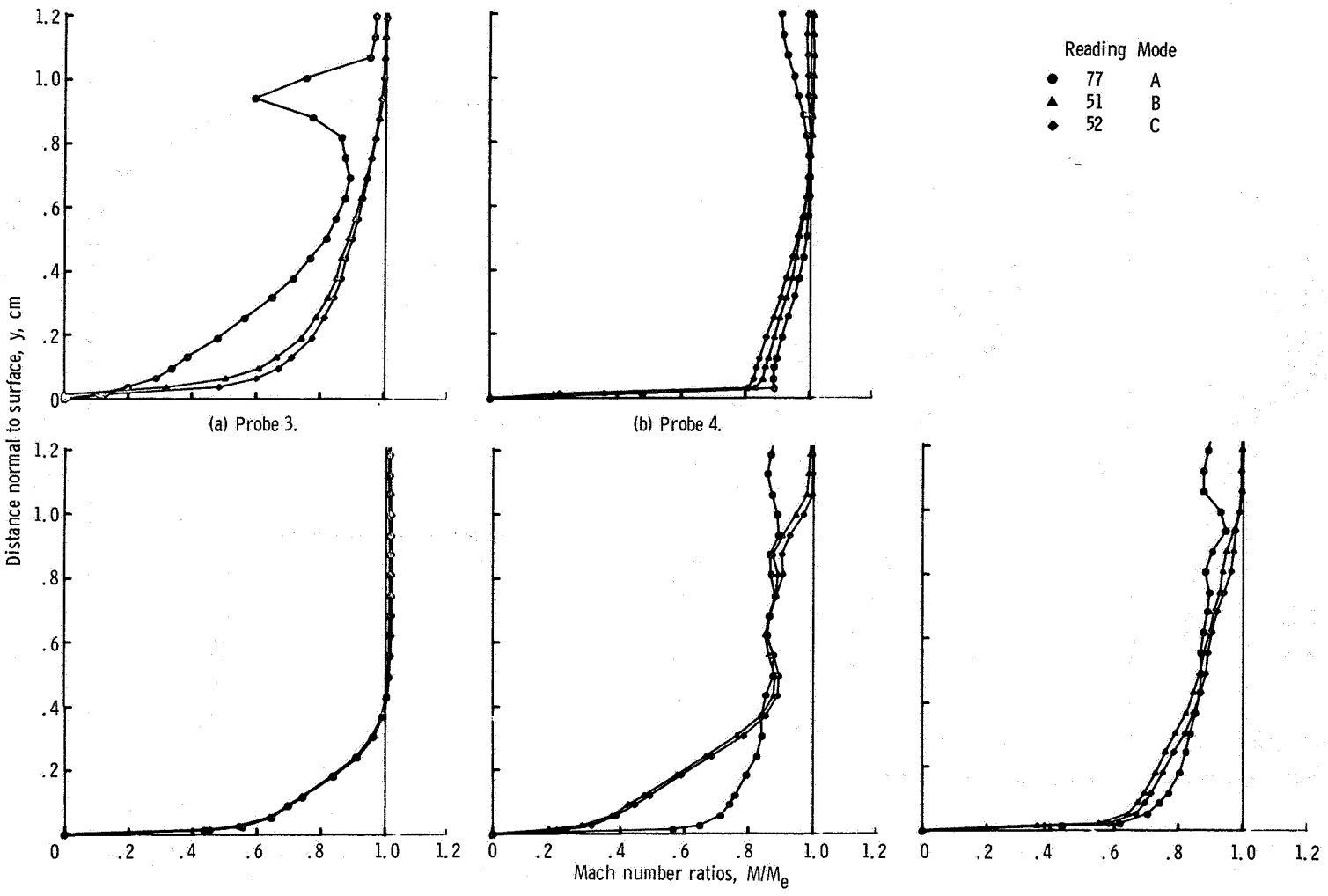

Figure 12. - Boundary-layer profiles for configuration US. Reynolds number per meter, 2.7×10^6.

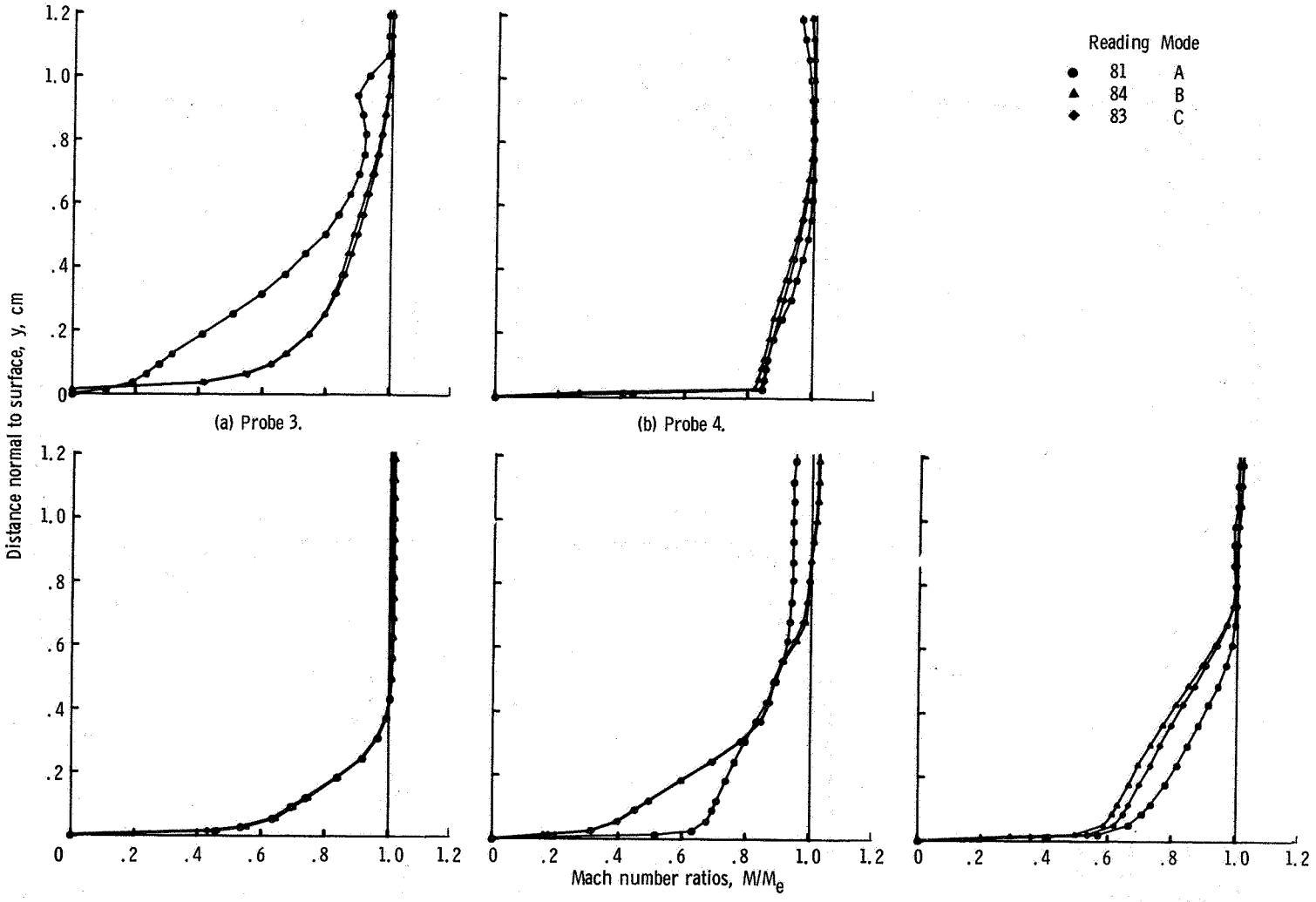

Figure 13. - Boundary-layer profiles for configuration AS. Reynolds number per meter, 2.7×10^6.

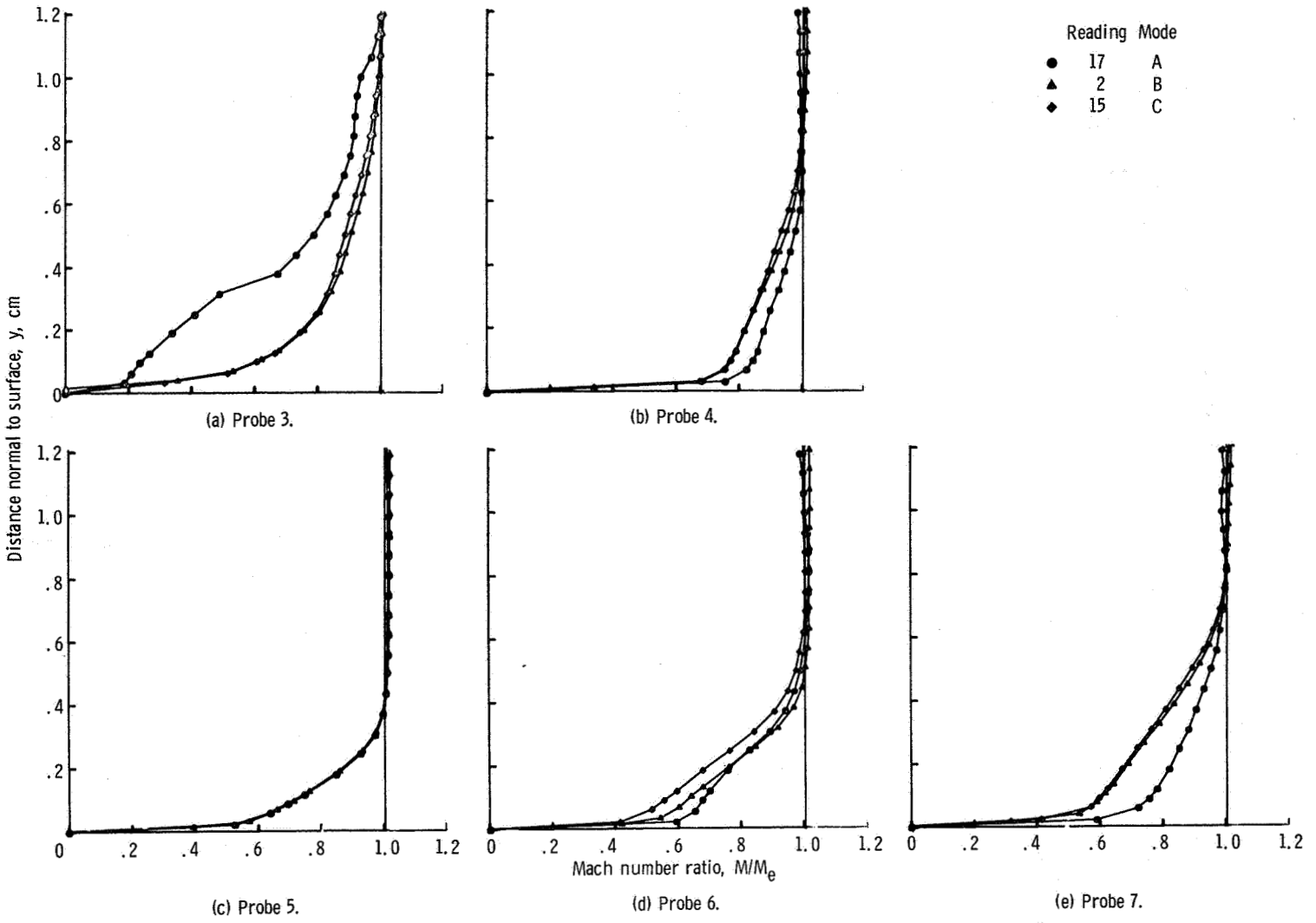

Figure 14. - Boundary-layer profiles for configuration DS. Reynolds number per meter, 2.7×10^6.

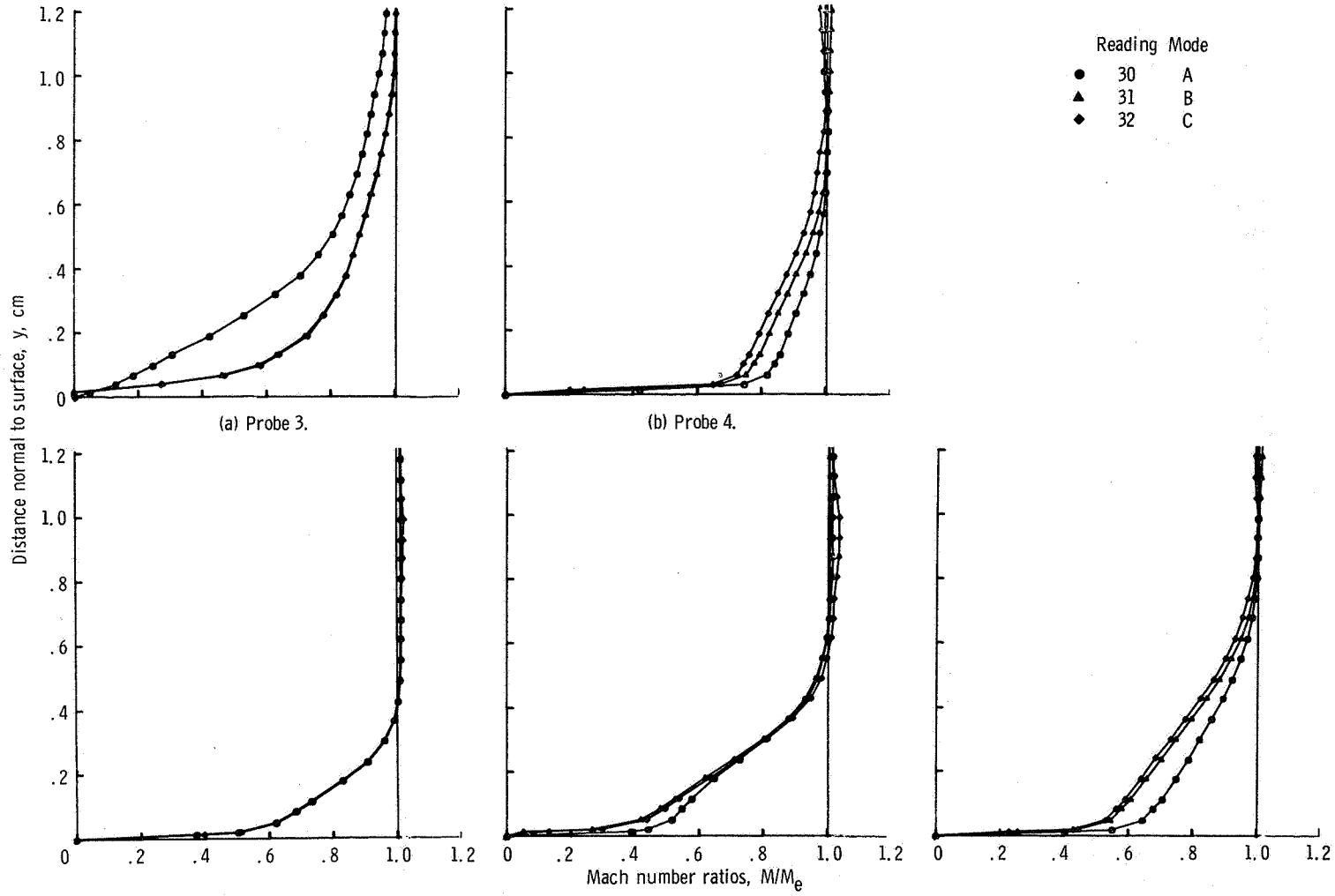

Figure 15. - Boundary-layer profiles for configuration DS I. Reynolds number per meter, 2.7×10^6.

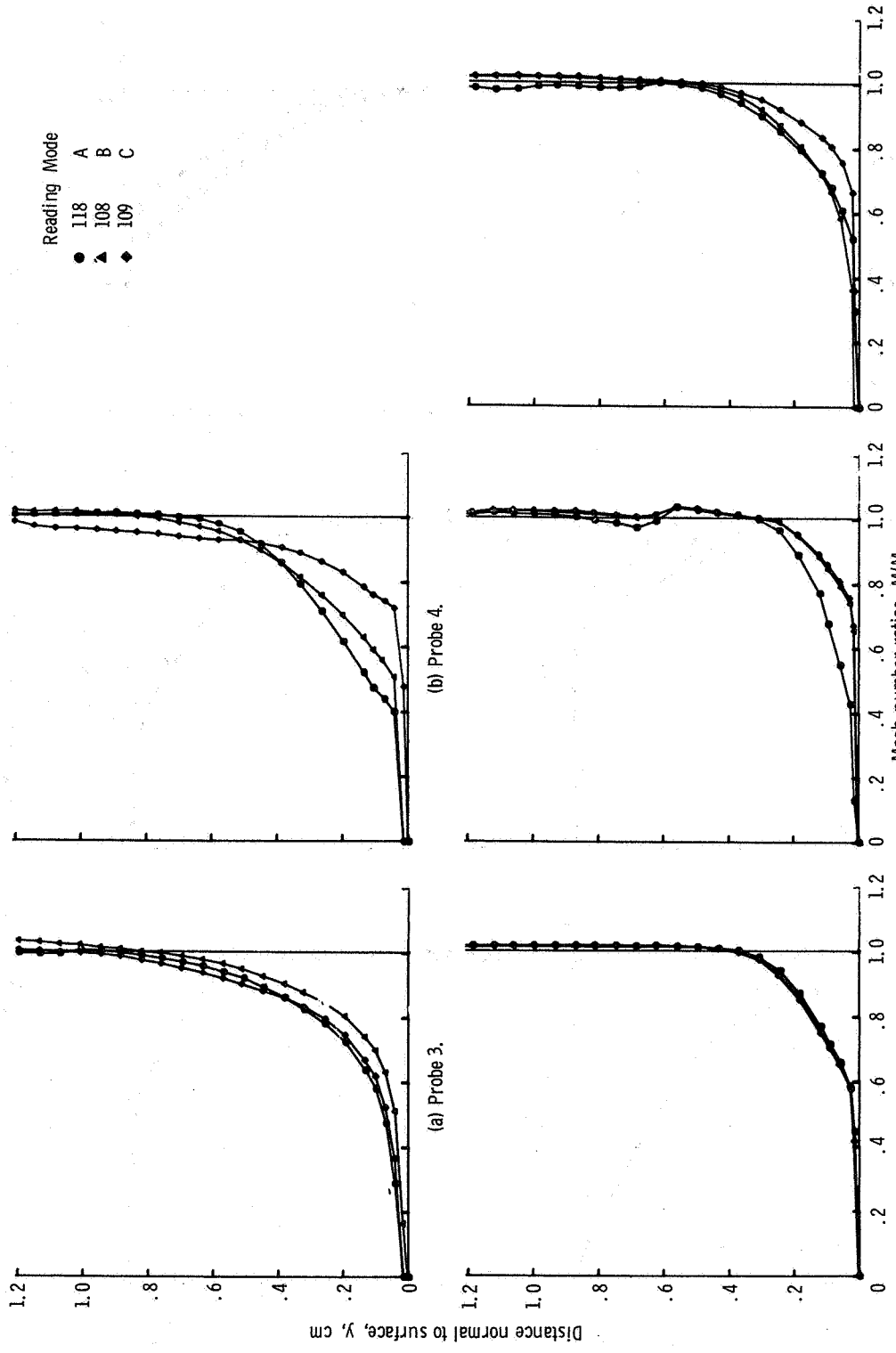

Figure 16. - Boundary-layer profiles for configuration DS III. Reynolds number per meter, 2.7×10^6.

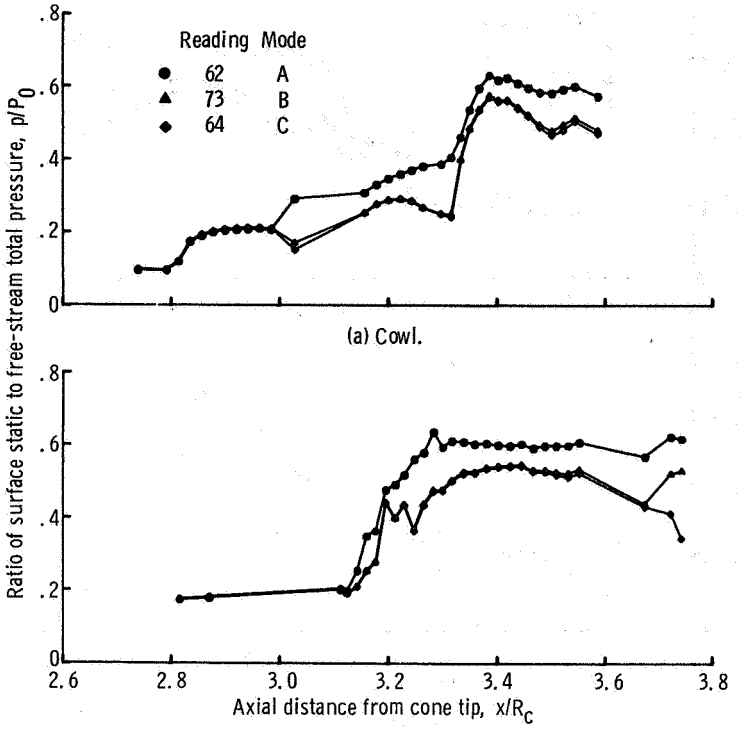

(a) Cowl.

(b) Centerbody.

Figure 17. - Static-pressure distribution for configuration US. Reynolds number per meter, 8.2×10^6.

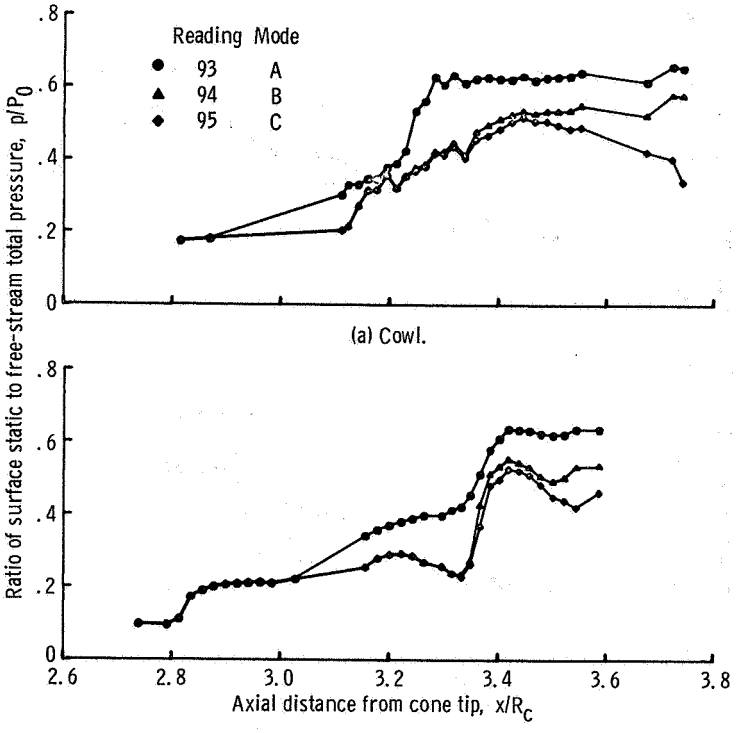

(a) Cowl.

(b) Centerbody.

Figure 18. - Static-pressure distribution for configuration AS. Reynolds number per meter, 8.2×10^6.

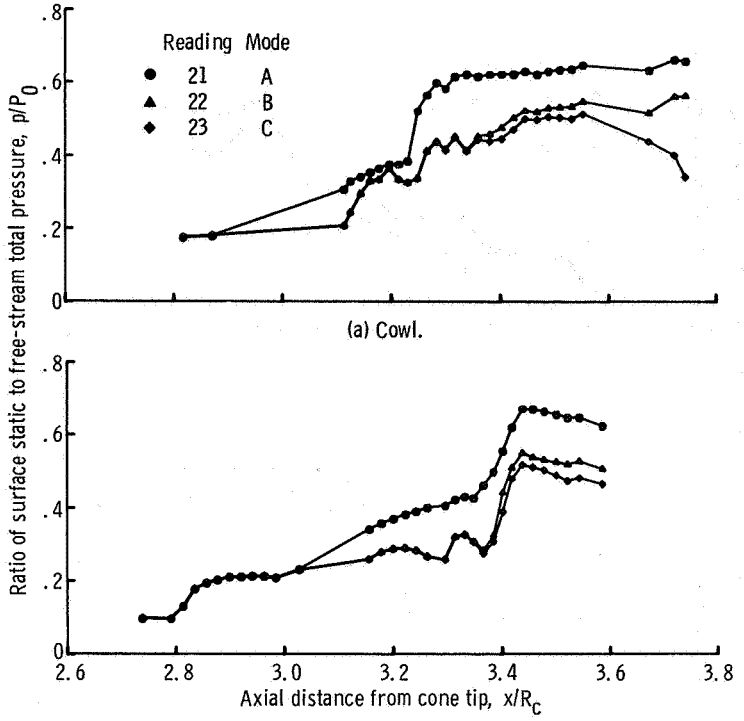

Figure 19. - Static-pressure distribution for configuration DS. Reynolds number per meter, 8.2×10^6.

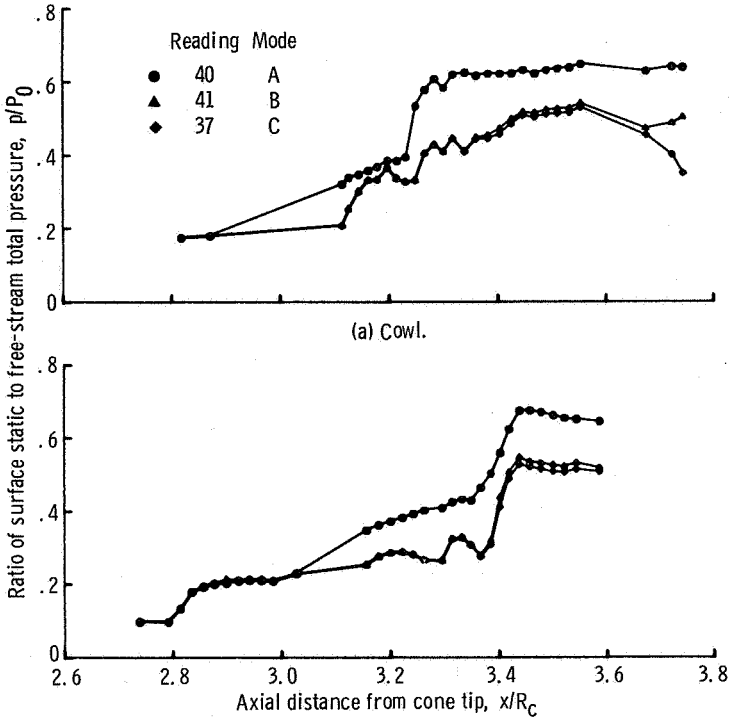

Figure 20. - Static-pressure distribution for configuration DS I. Reynolds number per meter, 8.2×10^6.

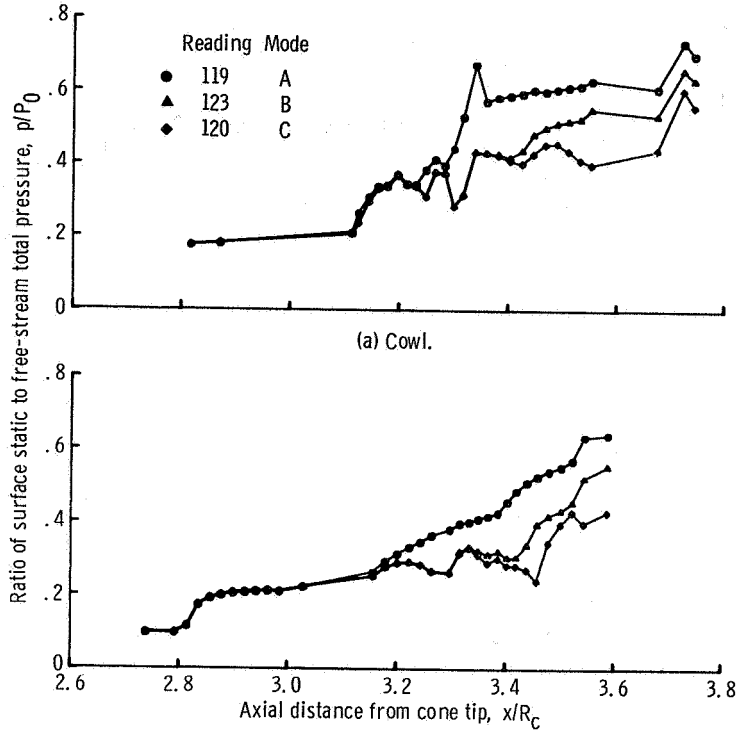

(a) Cowl.

(b) Centerbody.

Figure 21. - Static-pressure distribution for configuration DS III. Reynolds number per meter, 8.2×10^6.

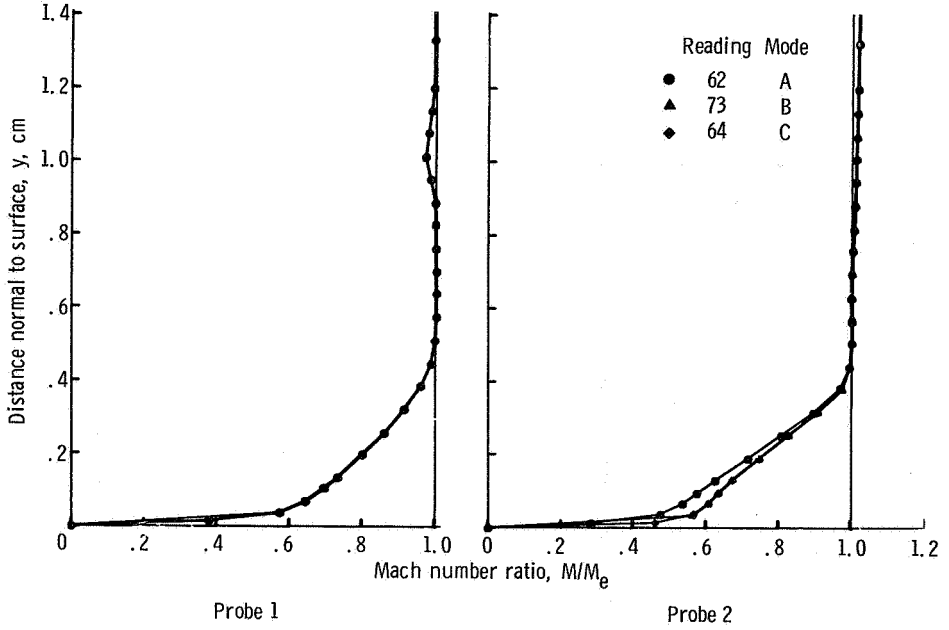

Figure 22. - Boundary-layer profiles for all bleed configurations. Reynolds number per meter, 8.2×10^6.

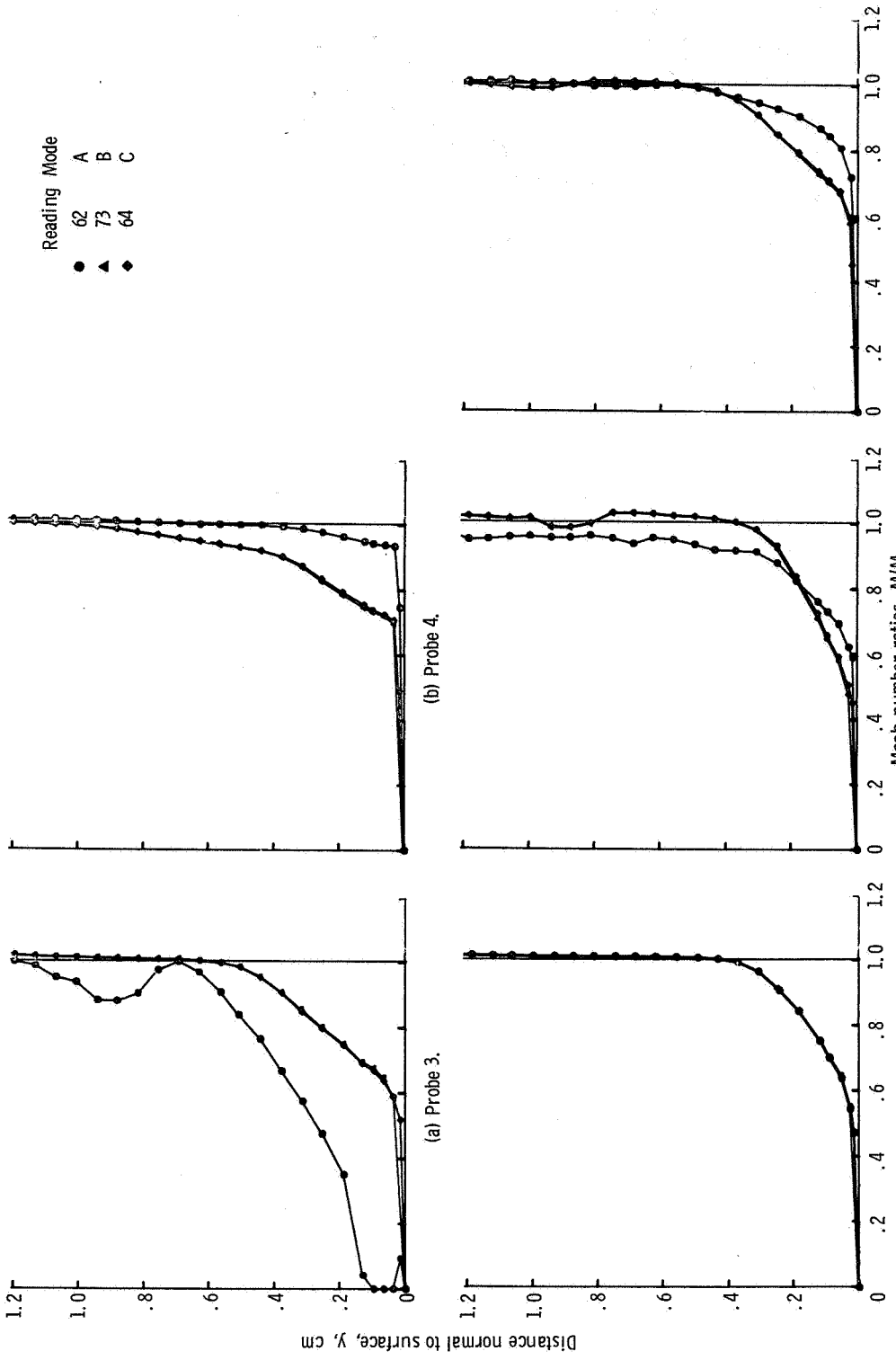

Figure 23. - Boundary-layer profiles for configuration US. Reynolds number per meter, 8.2×10^6.

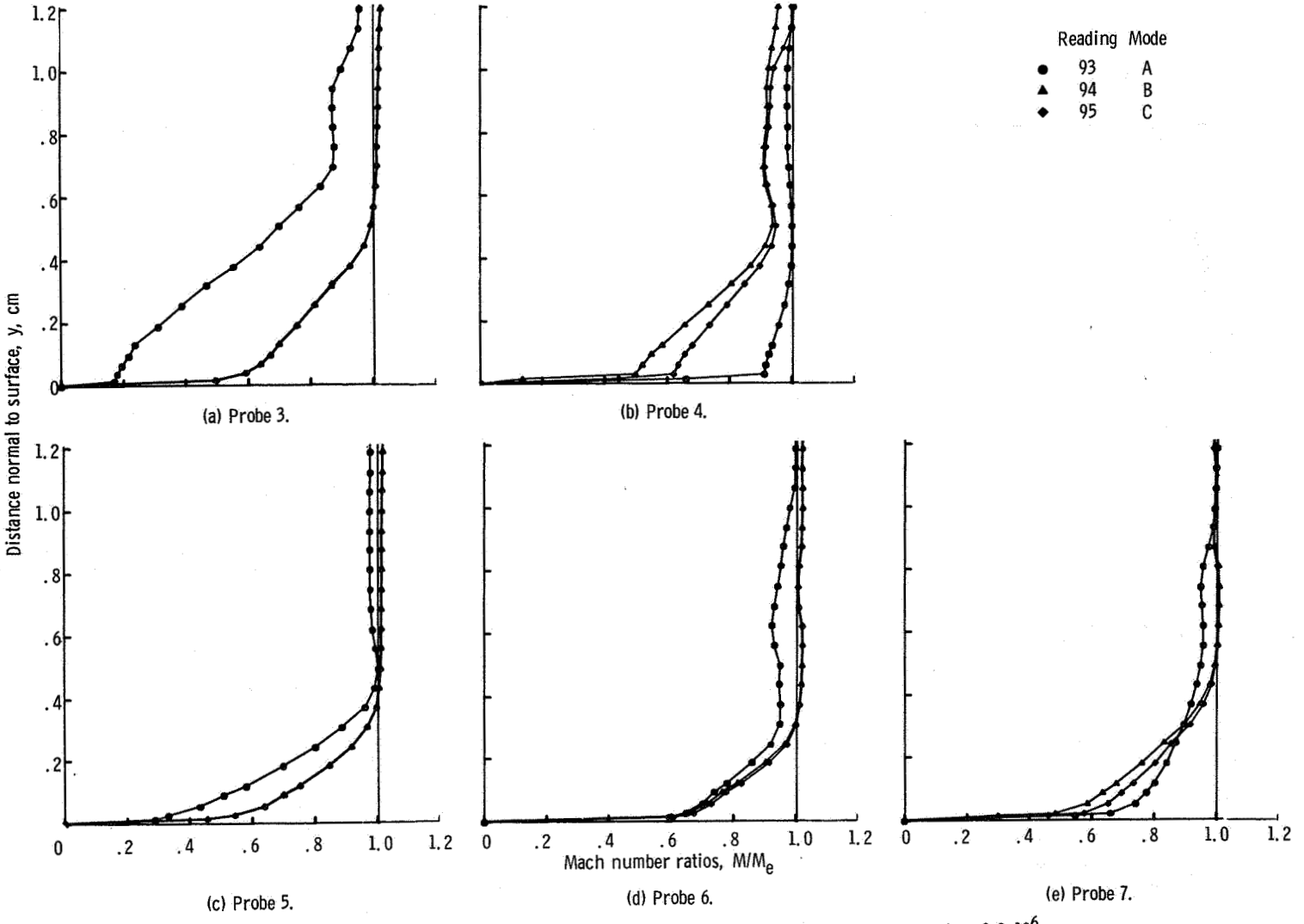

Figure 24. - Boundary-layer profiles for configuration AS. Reynolds number per meter, 8.2×10^6.

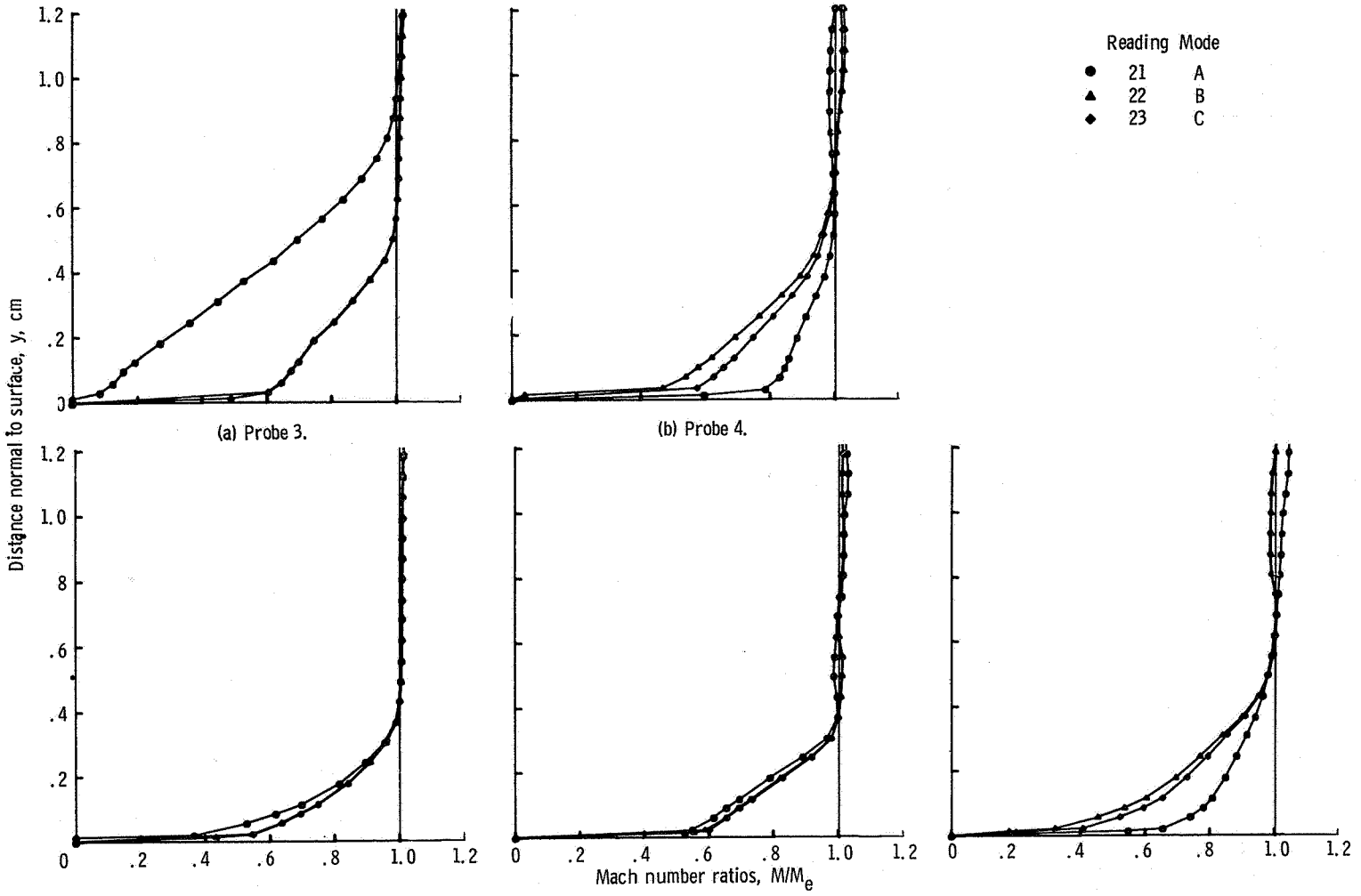

Figure 25. - Boundary-layer profiles for configuration DS. Reynolds number per meter, 8.2×10^6.

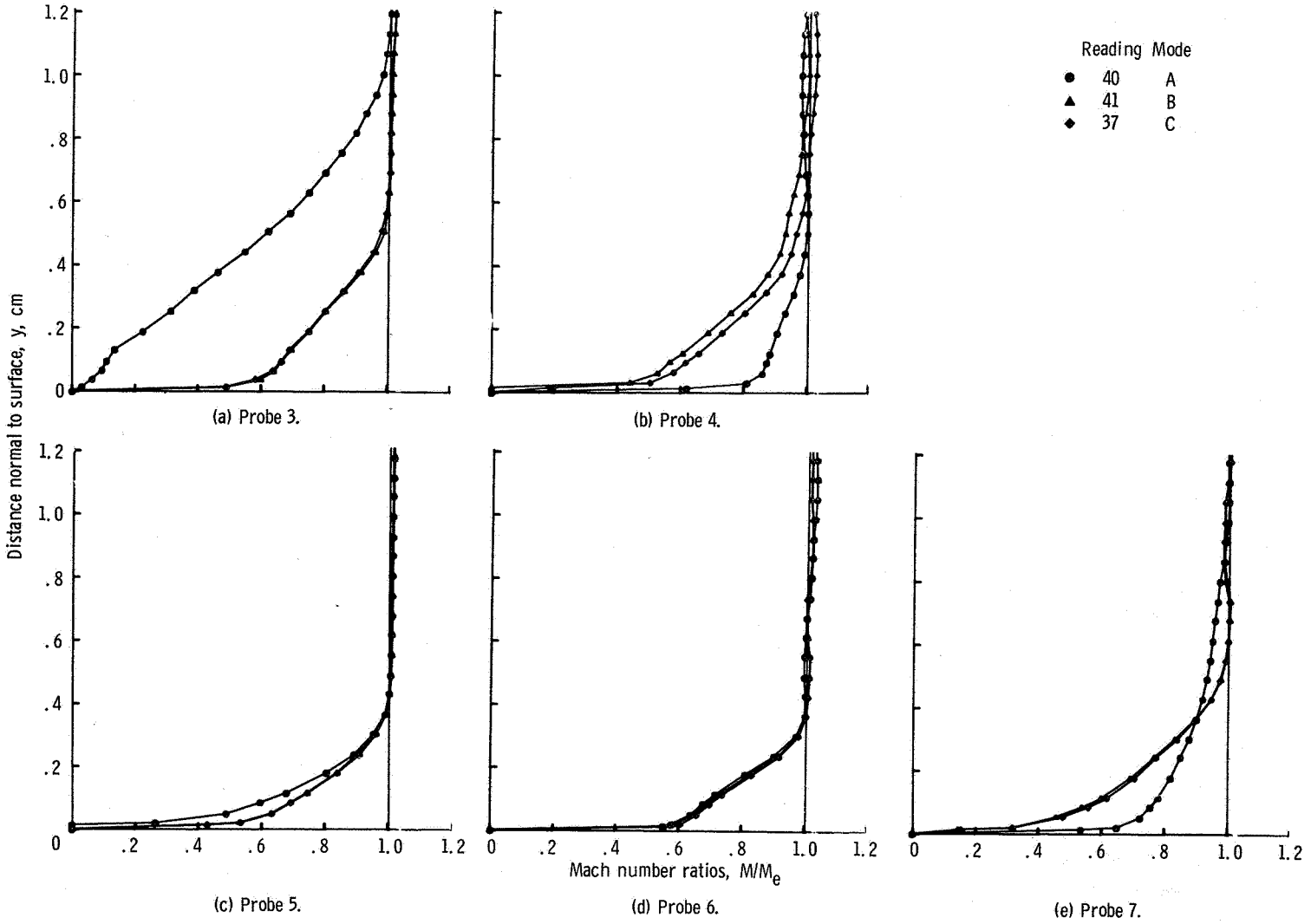

Figure 26. - Boundary-layer profiles for configuration DSI. Reynolds number per meter, 8.2×10^6.

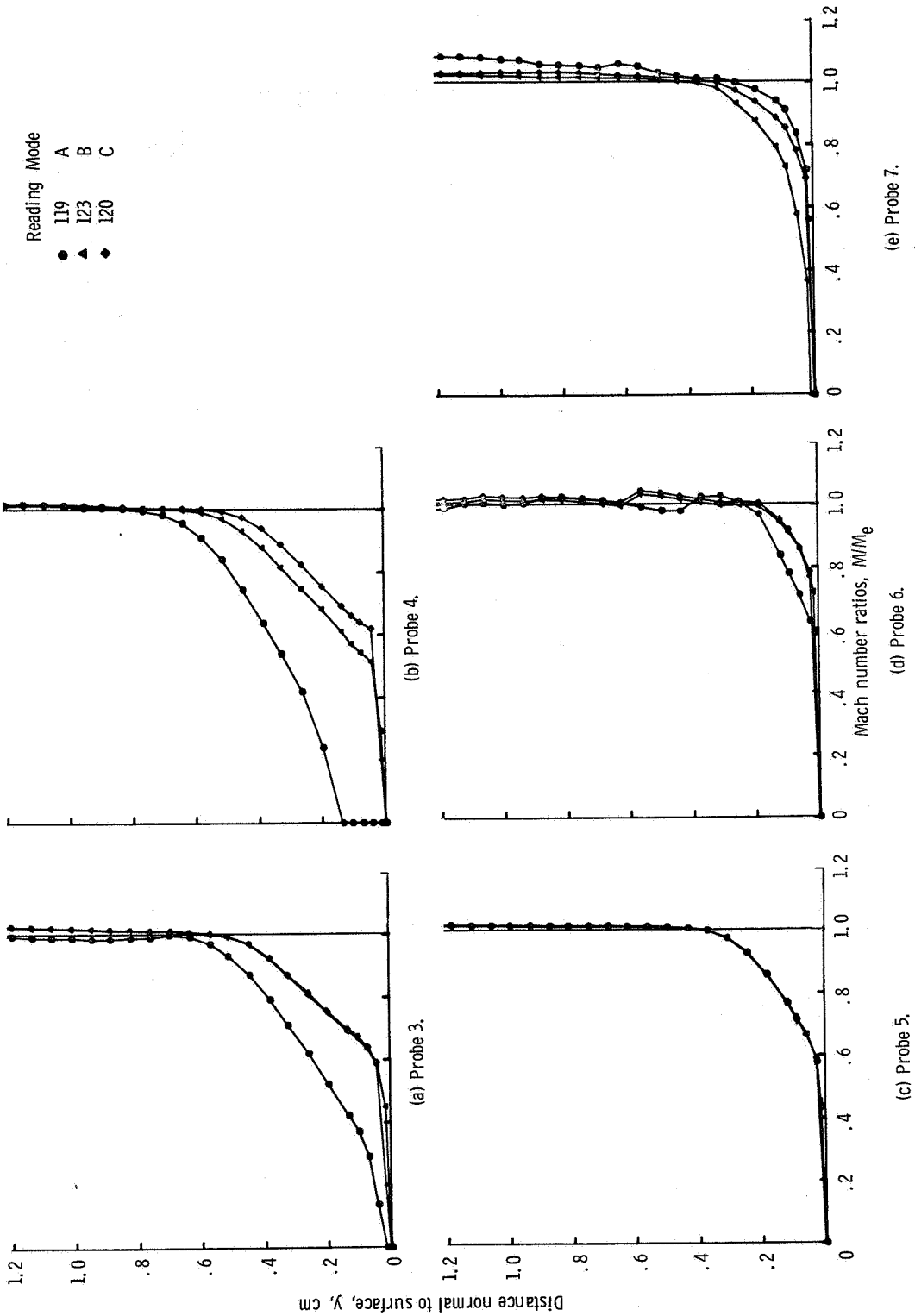

Figure 27. - Boundary-layer profiles for configuration DS III. Reynolds number per meter, 8.2×10^6.

NASA-Langley, 1973 —— 1